ShakeAlert® Version 3, Expected Performance in Large Earthquakes

Jeffrey J. McGuire[1*], Carl W. Ulberg[2], Angie I. Lux[3], Maren Böse[4], Jennifer R. Andrews[5], Deborah E. Smith[6], Brendan W. Crowell[2], Jessica R. Murray[1], Ivan Henson[3], Renate Hartog[2], Claude Felizardo[7], Minh Huynh[6], Mario Aranha[3], Grace A. Parker[1], Annemarie Baltay[1], Mark H. Murray[1], Glenn P. Biasi[6], Steve Guiwits[6], Jessie K. Saunders[7], Andrew D. Good[7], V. Marcelo Santillan[8], Craig W. Scrivner[8], Walter M. Szeliga[8], Timothy I. Melbourne[8], Victor Kress[2], Robert M. de Groot[6], Sara K. McBride[9], Douglas Given[6], Richard M. Allen[3], Thomas H. Heaton[7], Allen Husker[7], Valerie Thomas[6], Harold J. Tobin[2], Sumant Jha[1], and Julian Bunn[7]

[1] United States Geological Survey (USGS), Moffett Field, California, United States
[2] University of Washington (UW), Seattle, Washington, United States
[3] UC Berkeley Seismological Laboratory (UCB), Berkeley, California, United States
[4] Swiss Seismological Service (SED), ETH Zürich, Switzerland
[5] GNS Science, Lower Hutt, Wellington, New Zealand
[6] United States Geological Survey (USGS), Pasadena, California, United States
[7] California Institute of Technology (Caltech) Seismological Laboratory, Pasadena, California, United States
[8] Central Washington University, Ellensburg, Washington
[9] United States Geological Survey (USGS), Golden, Colorado, United States

* Corresponding author: U.S. Geological Survey, Earthquake Science Center, 345 Middlefield Rd. Menlo Park CA 94035; jmcguire@usgs.gov

Abstract:

The ShakeAlert® Earthquake Early Warning (EEW) system partners along with U.S. Geological Survey (USGS) licensed operators deliver EEW alerts to the public and trigger automated systems when a significant earthquake is expected to impact California, Oregon, or Washington. ShakeAlert's primary goal is to provide usable warning times before the arrival of damaging shaking. EEW is most likely to achieve this goal in large magnitude earthquakes. In recent years, ShakeAlert has gone through a series of upgrades to its underlying scientific algorithms aimed at improved performance during large earthquakes. Version 3 of this software recently went live in the production system and includes improvements to all algorithms. The main seismic algorithms which detect an earthquake and characterize its location, magnitude and fault rupture orientation are faster than older versions. Other key changes include: using real-time geodetic data to characterize the magnitude growth in large earthquakes; the introduction of an Alert Pause procedure to compromise between speed near the epicenter and improved accuracy at larger distances; and the inclusion of a non-ergodic site response model in the ground motion predictions. ShakeAlert has achieved its primary goal of usable warning times before strong shaking at some locations in real-time operations in recent M6 earthquakes. Using offline tests, we demonstrate usable warning times are possible for many sites with peak shaking values of Modified Mercalli Intensity (MMI) 7-8 in M7+ earthquakes and also for many MMI 8-9 sites in M8+ earthquakes. ShakeAlert partners use a variety of MMI and magnitude thresholds in deciding when to alert their users within bounds set by the USGS. Our study shows that there is room to raise the magnitude thresholds up to about M5.5 without adversely affecting performance in large earthquakes. The ground motion criteria are more complex owing to a significant drop-off in warning times between the MMI 4 and 5 levels of predicted shaking. However, widely used ShakeAlert products, such as the MMI 3 and 4 contour products, can provide sufficiently long warning times before strong shaking in moderate to great earthquakes to enable a range of protective actions.

1. Introduction

The ShakeAlert® Earthquake Early Warning (EEW) system (ShakeAlert system, ShakeAlert EEW, ShakeAlert) for the U.S. West Coast is operated by the United States Geological Survey (USGS) in partnership with academic and industry partners [Given et al., 2014; Given et al., 2018; Kohler et al., 2020]. The fundamental mission of ShakeAlert has always been: “to reduce the impact of earthquakes and save lives and property in the United States by developing and operating a public EEW capability" [Given et al., 2014]. The technical details of how this mission statement has been pursued have evolved over a decade-long development process. On March 18th, 2024, version 3.0.1 of the ShakeAlert system software (here after V3) went live for alerting in CA, OR, and WA [USGS, 2024]. V3 is the result of a significant series of upgrades with the goal of enabling better performance during large earthquakes including being the first version of the ShakeAlert system to utilize geodetic data. Performance of the real-time production system during recent small to moderate earthquakes has been detailed by Lux et al. [2024]. Here we describe the recent changes to the contributing algorithms and the expected performance of the system in future earthquakes.

ShakeAlert has a modular design that combines a complimentary set of algorithms that use different types of ground motion data and estimate source parameters and an algorithm that uses those parameters to estimate expected ground motions [Kohler et al., 2020]. The ShakeAlert system consists of four processing steps (Figure 1): 1) algorithms that process incoming seismic or Global Navigation Satellite System (GNSS) data, 2) algorithms that estimate source parameters, 3) an algorithm that combines parameter estimates and an algorithm that estimates maximum shaking levels given those source parameters, and 4) a decision module that issues ShakeAlert's data product (a ShakeAlert Message) if certain magnitude and intensity criteria are met. The algorithms used in V3 are termed EPIC [Kuyuk et al., 2014; Chung et al., 2019], FinDer [Böse et al., 2012, 2015, 2018, 2023a], GFAST-PGD [Crowell et al., 2016; Murray et al., 2023] for estimating source parameters, EqInfo2GM [Thakoor et al., 2019] for estimating shaking levels, the Solution Aggregator (SA), and Decision Module (DM) [Kohler et al., 2020] for combining source parameters and issuing the ShakeAlert Messages. EPIC uses observations of the initial P-waves to estimate the epicenter point-source parameters: latitude, longitude and magnitude, while FinDer uses evolving estimates of peak acceleration of the entire time series to estimate a line source that characterizes a growing rupture, and GFAST-PGD estimates only the magnitude using (geodetic) peak ground displacement (PGD) observations given an epicenter location from the seismic algorithms (EPIC and FinDer). The SA and DM are the same algorithm with different configuration parameters for forwarding on solutions.

ShakeAlert's modular design allows it to take advantage of different portions of the deformation field from a growing rupture, as will be described below, to maximize performance. It also offers some degree of redundancy, by using different data types and approaches, increasing resilience of the overall system to unexpected/sub-optimal behavior in some component. However, this comes at the cost of notable system complexity, which increases the challenges of maintenance and modification. However, many global EEW systems, including ShakeAlert, are continuing to evolve in response to new technologies, maturing performance expectations, and increasing real-time earthquake experience. So, while system simplicity is appealing for a number of reasons, and will hopefully be achievable in the future, no single approach has yet proven itself to meet all targets for desired behavior. Additionally, the modular design allows initial alerts to be issued before a large rupture is finished while also tracking the full extent of rupture/fault growth with more appropriate methods.

ShakeAlert Version 3 aims to improve performance of the system, and documenting those improvements requires a detailed articulation of ShakeAlert's goals. A key early decision was that ShakeAlert would work with USGS licensed operators to provide public alerts and "information rich alert streams to specialized users" [Given et al., 2014]. A Licensed Operator (LtO) is a ShakeAlert technical partner that is licensed by the USGS to provide ShakeAlert-powered products and services such as alert delivery to the cell phones or the triggering of an automated action like slowing a train. Owing to the flexibility needed to accommodate a range of applications, ShakeAlert required quantitative forecasts of expected ground motions from MMI 2 to 8 rather than simply spatial alert maps [Given et al., 2014]. ShakeAlert's quantitative objectives began to crystalize with the Revised Technical Implementation Plan [RTIP, Given et al., 2018] that emphasized two classes of performance defined by 1) accuracy of ShakeAlert's earthquake location and magnitude estimates relative to the point-source parameters of the Automated National Seismic System's (ANSS) Comprehensive Catalog (ComCat; USGS, 2017) and 2) the comparison of ShakeAlert's predicted ground motions with the spatially smooth model of ground motions provided by the USGS ShakeMap product [Worden et al., 2020; Given et al., 2018]. While the mission statement clearly requires sufficient warning times to enable people to take a protective action such as Drop, Cover, and Hold On (DCHO) and to complete triggering of automated actions, this was not yet formulated as a quantitative goal [Given et al., 2018]. This resulted for many reasons including that the system was not yet constructed, the algorithm base was rapidly evolving, and the full variety and speed of delivery mechanisms was relatively unknown. The RTIP provided clear definitions of ShakeAlert's three primary products: 1) an Event Message containing source parameters; 2) a Contour Message that provided 8-sided polygons that enclosed regions of different levels of shaking ranging from 2 to 8 on the Modified Mercalli Intensity (MMI) scale and associated peak ground acceleration and peak ground velocity values; and 3) a Map Message that provides a spatial grid of estimates of peak ground acceleration, velocity, and MMI level. The Contour and Map products were to both resemble and be compared to the median shaking estimates from the USGS ShakeMap product [e.g. Figure 8 of Given et al., 2018]. Currently, the MMI 3 contour product is defined as the distance at which median shaking is expected to be MMI

2.5, and similarly for the higher MMI contour products (see Section 2.3 below). ShakeAlert's original emphasis on a direct comparison to the ShakeMap product led to the specification that ShakeAlert's goal was the same at all locations, namely accurate ground-motion predictions as quickly as possible. Thus, from its inception, ShakeAlert has prioritized ground motion accuracy over a wide range of shaking levels from MMI 2 to 8.

Given these product definitions, ShakeAlert allows technical partners who have met the requirements for a license to distribute ShakeAlert-powered alerts to their end-users [Kohler et al., 2020]. ShakeAlert has always been specifically designed to allow a wide range of customization in how licensed operators implement alert delivery. However, USGS, in collaboration with state emergency management agencies in California, Oregon, and Washington, has set minimum alert delivery thresholds for both the magnitude estimate and expected shaking intensity in order for particular classes of delivery mechanisms to initiate alert delivery (Figure 2). For public alerting, there are three key sets of threshold criteria in wide use. ShakeAlert uses the Wireless Emergency Alert (WEA) system, and messages must meet the Federal Emergency Management Agency's (FEMA) criteria for 'imminent threat' [Federal Communications Commission, 2015]. Thus the thresholds were set to alert the MMI 4 area at a magnitude threshold of 5.0 or larger. In contrast, some cell phone apps, such as MyShake [Patel and Allen, 2022], send alerts for M 4.5+ and within the MMI 3 contour product corresponding to significantly larger areas and more frequent alerts [Kohler et al., 2020]. Lastly, Google's Android Earthquake Alerts uses a bi-level strategy with silent notifications (termed "Be Aware" alerts) at M4.5 and inside the MMI 3 contour product, but additionally augments these with loud break-through alerts (termed "Take Action" alerts) at M4.5+ within the MMI 5 contour product [Chung et al., 2020]. The different MMI and magnitude combinations lead to different frequencies of when a user will be alerted (see McGuire et al., 2021 for estimates for the Pacific Northwest based on the USGS National Seismic Hazard Model).

Moreover, these different delivery mechanisms have different ranges of latency that evolve as the underlying technology improves. For instance, the fastest deliveries are achieved over internet/WiFi systems allowing substantial numbers of users to receive the messages less than one second after USGS publishes them [McGuire and de Groot, 2021]. The MyShake™ app has documented delivery times in the 2-5 s range [Patel et al., 2022] for a combination of WiFi and cellular delivery. The WEA system does not have a recent test (e.g. after recent upgrades) but was documented to have delivery times ranging from 4 s to tens of seconds through cellular network delivery in 2019 [McBride et al. 2023]. WEA alerts are part of the Integrated Public Alert and Warning System (IPAWS) which uses both cellular and internet delivery for various alerts and is expected to adopt "future technology" to improve alerts [FEMA, 2024]. The technology for delivering earthquake alerts is rapidly evolving and improving [e.g. see Apple (2023)]. Thus, WEA message delivery may reach internet delivery speeds in the future. Overall, delivery times can range widely but many end users will receive the ShakeAlert Message within 0.5-5 s of when it is published by USGS.

Currently our licesnced operators take various actions at predicted MMI values ranging from MMI 2.5 to 5.5 [Chung et al., 2020; McGuire et al., 2021] to achieve their desired outcomes. Given the latitude that licensed operators have to choose alert thresholds (within a range established by the USGS), as well as the variable speed of different delivery mechanisms, ShakeAlert needs to produce products with a significant degree of accuracy across a wide MMI range.

ShakeAlert's primary objective is to provide usable warning times before strong (MMI 6+) shaking where it is possible to do so. The range of user locations, combined with the choice of alert thresholds and the variability in delivery times, results in a wide range of potential warning times in any given earthquake [Chung et al., 2020; McGuire et al., 2020; Lux et al., 2024]. The recommended protective action in most cases when receiving an alert is "Drop, Cover, and Hold On" or DCHO [see McBride et al., 2022] because injuries often occur when trying to move during strong shaking or by being hit by falling objects. It is expected that it will take end-users between 5 and 15 s to complete DCHO [Porter and Jones, 2018], so for ShakeAlert to achieve its primary objective, alerts need to be delivered to a location at least 5-15 s before damaging MMI 6 shaking begins. Longer warning times are obviously preferred and can enable a wider range of actions than just DCHO, including automated actions in mechanical systems. In general, ShakeAlert does not have location specific delivery time statistics for its different delivery mechanisms, and many evaluations are done with offline simulations that don't account for data telemetry and alert delivery latencies. In these types of simulations, which will be presented below, it is reasonable to assume that the combination of data telemetry and alert delivery adds a minimum delay of 2 s, and typically ~5 s, over what the algorithm processing time requires, acknowledging that many delivery mechanisms require at least a few seconds more than this nominal value. As a result, since the formal test of V.2.2.0 of the ShakeAlert software package in February 2022 (see table S1), ShakeAlert's testing and certification platform has used a metric that quantifies the fraction of MMI 6 locations (with observed seismic data) that achieve a minimum warning time of 8-10s in offline tests to track the system's ability to achieve its primary objective.

1.1 ShakeAlert system development history

To move towards its stated goals and to enable a wide range of delivery thresholds, ShakeAlert evaluated algorithm improvements using its system testing platform (STP) [Cochran et al. 2018] to identify modifications or new features that provide improved source parameter estimates and/or ground motion products [Kohler et al., 2018]. In particular, the development of the eqInfo2GM module formulated the initial version of ShakeAlert's ground motion predictions that are published as the Map and Contour products [Thakoor et al., 2019]. Thakoor et al. accomplished the RTIP strategy in that eqInfo2GM produces median shaking estimates that are equivalent to the USGS ShakeMap methodology of using ground motion prediction equations when no seismogram data are used, e.g. when only earthquake source parameters are available to predict shaking. Thakoor et al. used an evaluation scheme based on measuring the L2 norm of differences between predicted median shaking intensity estimates from eqInfo2GM to assess that the ShakeMap ground motion predictions were properly implemented. This metric, termed variance reduction, places the most weight on the larger number of lower MMI grid cells (regardless of any selected MMI threshold) in any given event and has been used in ShakeAlert system testing for that same purpose. Given these structures, the USGS ShakeAlert Project initially refined its algorithms via the STP process with its strong focus on matching the Advanced National Seismic System (ANSS) Comprehensive Catalog (ComCat, USGS, 2017) for small to moderate earthquakes [Cochran et al., 2018] and with ground motion metrics that focused primarily on the large number of MMI 2 and larger [Thakoor et al., 2019] or MMI 4 and larger [Cochran et al., 2018] grid cells in a typical ShakeMap. This preliminary focus on matching detections and magnitude estimates for moderate earthquakes succeeded in driving the system towards very low false alert rates [Kohler et al., 2018] which allowed it to begin public alerting in 2019 using Version 2.0 of the ShakeAlert software suite [Kohler et al., 2020]. The reduction in false alert rates due to the improvements leading up to ShakeAlert V2.0 combined with the build out of the seismic network and associated telemetry systems were significant accomplishments, and they provided a necessary condition to build trust in the system among both internal partners and the public. The result of these efforts was the launch of a test of the system for public alerting in Los Angeles County via cellphone apps on January 1, 2019, using an EEW app developed by the City of Los Angeles.

In July 2019, the ShakeAlert system received its first major test with the occurrence of the M6.4 and 7.1 Ridgecrest earthquakes in Southern California. The system faced a wide variety of challenges in these events ranging from a very productive sequence of moderate earthquakes/foreshocks/aftershocks, data telemetry problems [Stubailo et al., 2020], and algorithm combination approaches during the M7.1 mainshock [Chung et al., 2020]. The net result of these problems was that in locations where timing information was available from recorded seismograms, the ShakeAlert system provided no significant warning times for sites of MMI6+ shaking in the M6.4 earthquake. For the M7.1, about 25-30% of locations that experienced MMI 6 shaking could have received usable warning times (roughly 5-10 seconds before moderate/strong shaking, see discussion below). No sites with recorded shaking of MMI 7+ could have received usable warning times even with an instantaneous alert delivery mechanism [Chung et al., 2020]. While ShakeAlert did not achieve its primary objective at most locations of damaging shaking, the first alert was rapid given the sparse station spacing. It was the first real-time test of the system in a large earthquake and helped identify many areas for future improvement.

As a result of the performance of ShakeAlert V2 in the Ridgecrest mainshocks, the ShakeAlert Project undertook a major, years long effort to overhaul the underlying algorithm base and improve its performance in large earthquakes [Böse et al., 2023a; Böse et al., 2023b; Murray et al., 2023; Lux et al., 2024]. One key feature of our evaluation system that required upgrading was an increased focus on offline testing using large earthquakes. The original test suite that is used for evaluation of software upgrades in ShakeAlert was constructed before the station buildout for EEW and focused on publicly available data from the U.S. West Coast. As a result, the large earthquakes in it did not have a station density that represents the current or future operational network [Cochran et al., 2018], and ShakeAlert V2.0 had not yet identified problems tracking magnitude growth in large earthquakes [Kohler et al., 2020]. V2.0 was effectively hardwired to weight the magnitude estimates from the EPIC algorithm much more strongly than those from the FinDer algorithm during a large rupture [Kohler et al., 2020; Chung et al., 2020]. EPIC is a fast, specialized initial detection algorithm that only uses the first 4-5 seconds of P-wave data from any given station in its magnitude estimate. Because ShakeAlert V2.0 weighted this estimate disproportionately heavily even after much longer data streams with peak shaking values were available, ShakeAlert's magnitude estimate could not have reached M7.1 in the Ridgecrest mainshock even if the data telemetry had worked properly [Chung et al., 2020]. Since Ridgecrest, the ShakeAlert STP program has undergone a major overhaul that will be detailed elsewhere which includes a vastly expanded test suite. Additionally, alongside the original ANSS catalog-related metrics that penalize false alerts, we added two metrics that reward long warning times for sites of MMI6+ shaking and quantify/penalize over alerting at certain MMI levels (see below) used by USGS to activate the WEA system. The result of these additions has been to drive the system in the direction of improved performance in large earthquakes with a focus on locations where users are in potential danger, meaning MMI 6 or stronger shaking. For instance, in the 2022 M6.4 Ferndale earthquake, the ShakeAlert system provided between 0-12 s of warning at locations which experienced MMI 8 shaking, 0-17 s at MMI 7 locations, and 0-23 s of warning at MMI 6 locations [Lux et al., 2024].

ShakeAlert's increased focus on providing usable warning times in large earthquakes has resulted in V3, which was implemented on March 18th, 2024. This update allows the different source estimation algorithms to contribute predominantly in the earthquake magnitude ranges where they are most applicable with prescribed transitions based on significant offline testing in large earthquakes. V3 acknowledges the need to act quickly in the vicinity of the epicenter when accurate magnitude and ground motion estimates are more difficult to produce due to limited data, while also acknowledging the need for increased accuracy of shaking estimates at larger distances to limit over alerting. The overall suite of algorithm changes compared to V2 are both the cumulative result of dozens of intermediate modifications (see Table S1) as well as a fundamental change involving the incorporation of geodetic data and site response models for the first time. This paper describes those changes and their cumulative effect on expected performance in large earthquakes. ShakeAlert is an EEW system designed to "save lives and property" which fundamentally requires alert delivery before damaging strong shaking arrives. Timeliness is an absolute requirement for success of the ShakeAlert system, while detailed ground-motion accuracy is a helpful but less stringent requirement. Both timeliness and ground-motion accuracy depend to some extent on definitions, and this paper describes the state of the system in both regards from offline testing of V3.

The expanded STP test suite has a wide variety of earthquakes in terms of types of faults, geographic locations, station density, and an increasing number of synthetic earthquakes [Smith et al. 2024]. For this paper we will focus on results from three key subsets of the test suite which are the updated West Coast, Japan crustal, and Japan subduction zone components. The earthquakes used are listed in Supplementary Table 2. Many of the Japanese events were studied on an individual algorithm basis in Meier et al. [2020] and the geodetic events were studied for the GFAST-PGD algorithm in Murray et al. [2023]. To evaluate warning time, we follow the ShakeAlert standard practice by comparing alert times to the time the seismogram at a station exceeds a given MMI value similar to that used in Chung et al., [2020]. Defining the warning time requires specifying three quantities, the MMI level the alert is issued for (MMI_{alert}), the type of product (contour vs grid), and the MMI level that you want to be warned for (MMI_{tw}). MMI_{alert} and MMI_{tw} could be the same or MMI_{tw} could be larger, which generally leads to better warning time performance [Meier et al., 2017; Minson et al, 2018; Chung et al., 2020]. The warning time at a given site is the time between when it is first predicted to have shaking of at least MMI_{alert} and the time at which the observed shaking first exceeds MMI_{tw}. The expanded test suite provides a range of magnitude and distance combinations with peak shaking of MMI 6 or larger allowing warning times to be evaluated for a variety of cases (Figure S1). Because warning times are relatively short (seconds to tens of seconds) and the MMI_{tw} exceedance times can vary by a comparable amount of time even for stations at a similar epicentral distance, accurate algorithm evaluations require a seismogram to compute warning times with enough precision.

2. ShakeAlert 3.0

Of the six algorithms that comprise V3, only GFAST-PGD is new, but all six have been substantially modified from version 2.0. The key difference in ShakeAlert V3.0 vs ShakeAlert V2.0 is that V3.0 has separated the system into what is effectively four different regimes that correspond to increasing amounts of available data and larger earthquake sizes (see Table 1). Conceptually, these stages roughly correspond to 1) Initial detection, 2) Moderate Earthquakes, 3)

Large Earthquakes, and 4) Great Earthquakes. These are not formal divisions within the system; there is overlap between them and flexibility to follow different progressions based on the algorithm results during a given earthquake. In general, the progression is expected to emphasize EPIC initially, then FinDer, then a combination of FinDer and GFAST-PGD as a rupture grows in size up to M7+ (Figure 3). However, that is not always the case, and the logic is flexible enough to allow a particular algorithm to increase the magnitude estimate rapidly if its data type (see Table 1) warrants that increase. All three algorithms estimate source parameters that are combined by the SA. The transitions in emphasis between the algorithms are accomplished by logic that is embedded in the executive functions of the Solution Aggregator, EqInfo2GM, and Decision Module algorithms (Figure 3). The result of this logic is a system that emphasizes each algorithm for the magnitude and time range during the rupture for which it is most accurate and valuable (Table 1). In a truly great earthquake, there will be a series of transitions, described below, in how earthquake magnitude and predicted ground motions are estimated as the rupture grows. This progression takes into account our experience from real-time and offline testing in order to best utilize the different algorithms.

2.05 Current architecture and data flow

The data flow architecture for seismic data in V3 remains largely unchanged from earlier versions [Kohler et al., 2018, 2020]. Approximately 1400 seismic stations from a variety of seismic networks (network codes AZ, BC, BK, CC, CE, CI, CN, IU, NC, NN, NP, NV, OO, SB, UO, US, UW, and WR, see Data Availability statement) contribute data to ShakeAlert from either broadband and/or strong-motion seismometers. The seismic network is rapidly approaching the original system design target [Given et al., 2018] which features the highest density of stations in major urban areas and along major faults (Figure 4A). All seismic data flow to one of four seismic network processing centers (Caltech, UC Berkeley, USGS Moffett Field, and Univ. of Washington), is injected into the Earthworm system [Friberg et al., 2010; Hartog et al., 2020] and read by one of two waveform processing algorithms that produce parametric data for EPIC and FinDer. All parametric data are passed between the 8 production servers (2 per network center) using the Apache ActiveMQ open-source messaging broker software [Snyder, 2011]. Each algorithm subscribes to certain ActiveMQ topics for input and publishes results to other topics.

ShakeAlert uses data from continuously operating Global Navigation Satellite System (GNSS) stations distributed throughout California, Oregon, and Washington which are part of several monitoring networks. Approximately 1100 stations are potential ShakeAlert contributors, and at any given time ~950 stations are actively providing data to the ShakeAlert system (Figure 4B). Each station's data are telemetered in real-time to its respective network operations center which, in turn, provides real-time raw data streams to users. ShakeAlert uses a cloud-based data architecture for GNSS data operated by the EarthScope Consortium, which gathers the raw real-time streams provided by network operators for each station (including those from stations operated by EarthScope) and makes these available via a messaging system (Apache Kafka; Sax, 2018) to data processing center(s). Currently ShakeAlert has one data processing center, at Central Washington University (CWU), where one sample-per-second three component (north, east, vertical) real-time positions are estimated from the raw 1 Hz data using the Fastlane software [Santillan et al., 2013; Melbourne et al., 2021]. These real-time position streams are then transmitted in geoJSON format [Butler et al., 2016] via RabbitMQ messaging [Dossot, 2014] from CWU to ShakeAlert centers and are stored on Earthworm ring buffers [Friberg, 2010]. Once it is triggered by the first alert message issued by the Solution Aggregator (based on seismic data), the

GFAST-PGD algorithm then reads the epoch-by-epoch positions from the Earthworm ring. Efforts are underway to transition from using ring buffers to an approach in which GFAST-PGD obtains the real-time position streams via a messaging system.

The largely independent telemetry systems for the GNSS and seismic data provide a form of redundancy for ShakeAlert. In the 2019 Ridgecrest M7.1 mainshock, the GNSS position streams calculated by CWU using the Fastlane software did not experience any unusual data latencies and allowed accurate near real time magnitude calculations [Melgar et al., 2019; Hodgkinson et al., 2020] in contrast to the telemetry delays experienced by the ShakeAlert seismic systems [Stubalio et al., 2020]. While the GFAST-PGD algorithm requires a seismic algorithm event detection to begin calculating in the V3 software, it can keep updating regardless of the seismic algorithm performance (see below). Thus, the independent data telemetry pathway potentially provides a redundant aspect that could insulate ShakeAlert against the type of problems seen in Ridgecrest.

2.1 Initial detection

The initial detection of an earthquake in ShakeAlert V3 almost always comes from the EPIC algorithm, which utilizes P-wave arrival times from a minimum of 4 stations to estimate the epicentral latitude, longitude, and magnitude [Chung et al., 2019]. For crustal (depth <~20 km) earthquakes in densely instrumented parts of the ShakeAlert network, this first alert is typically published within about 4-6 seconds after the earthquake origin time [Lux et al., 2024]. After the Ridgecrest earthquakes, the EPIC magnitude estimation algorithm was updated to use a weighting scheme that gives preference to the stations with the longest duration of P-waveform available [Lux et al., 2024]. In the initial detection, this approach can result in one or two of the four stations having significantly higher weights than the remaining 2 or 3. This change was made to mimic the fundamental properties of P-waves which are proportional to the earthquake's moment-rate history. Also, it allows the initial magnitude estimate to grow more quickly in large earthquakes for which combining stations with ~4 seconds of data with stations that have less than a second of available data would otherwise bias the magnitude estimates to low values, as was the case with ShakeAlert V2 during the Ridgecrest mainshocks [Chung et al., 2020]. Additionally, the EPIC magnitude was constrained to be less than M7.5 due to the 4-5 second limit on available P-wave data [Trugman et al., 2019] whereas in V2, EPIC had been coded to allow magnitude estimates up to 10.0.

The new EPIC weighting scheme increases the sensitivity to stations with unusually large P-wave displacements for their magnitude and to the effect of mislocation in the initial epicenter estimate which affects the magnitude calculation. The weighting change combined with the inherent scatter in early magnitude estimates has been shown in testing to lead to systematic overestimates. Figure 5 shows the net positive bias in the peak magnitude estimate for V3 with the West Coast test suite and recent real-time results in California (see Figure S2 for Japanese event test results). While the DM estimates often eventually converge to a value closer to the ANSS catalog magnitude as more data become available, the peak magnitude estimate still controls the alert area. To counteract this effect to some degree, ShakeAlert coupled the adoption of the new EPIC magnitude weighting scheme with the introduction of an Alert Pause procedure defined by a pause radius and pause time that limit the geographic extent of the initial alerts. For V3 the pause radius is set to 100 km and the pause time is set to 5 s. These values were chosen based on real-time system performance in 2021 and 2022 and may need to be revisited in the future For the first alert and up to 5 seconds after the initial alert, the EqInfo2GM module will restrict any of the published contour products or map product grid cells to not have a radius larger than 100 km from the epicenter or finite fault estimate (if available). After the 5 s mark is reached, the ground motion products corresponding to the most recent alert update are sent out to their full spatial extent, and any additional alert updates will not have restrictions on their spatial extents. While ShakeAlert data products have always been defined as providing the best estimate of median expected ground motions in a given region [Given et al., 2014, 2018; Thakoor et al., 2019], it is recognized that uncertainties in the source parameters and the derived ground-motion estimates are much higher in the initial solutions (ShakeAlert Messages), yet for locations near the epicenter we must publish alerts quickly if they are to be useful. The Alert Pause logic is effectively a compromise between speed and accuracy. As a result of this strategy and the bias in peak magnitudes, it is more likely for the ShakeAlert system to produce overestimates of expected shaking inside the pause radius than outside it because after the 5 s have elapsed there are more data available to improve shaking estimates.

The pause radius limited alert distribution during several recent moderate earthquakes including the 2023 M5.1 Ojai CA, the 2023 M5.5 Prattville CA, and 2024 M4.8 El Centro CA earthquakes, correctly reducing the amount of over alerting in highly populated areas. In these cases, EPIC's initial magnitude estimate was produced with a small number of stations and in some cases suboptimal station geometry due to mountainous areas and incomplete station buildout. For the May 11th, 2023, Prattville earthquake the first magnitude estimate from the SA was M6.4, but by 5 s after the first alert the magnitude estimate had been reduced to M5.5. Similarly, in the August 20th, 2023, Ojai earthquake the first magnitude estimate was M6.0, but by 5 s later the magnitude estimate had been reduced to M5.7 [Lux et al., 2024]. In the Prattville case, the Alert Pause prevented Wireless Emergency Alerts frombeing sent to Sacramento unnecessarily. In the Ojai case, the Alert Pause prevented MMI 3 cell phone application alerts from being sent to San Diego, Fresno, and Salinas (Figure 6A). Additionally, MMI 4 alerts were prevented to the eastern half of Los Angeles. Similarly, for the February 12th, 2024, M4.8 El Centro earthquake, the initial SA/DM magnitude was M5.8 which was reduced to M5.5 by the 5 second mark. Without the Alert Pause, the initial MMI 3 alerts would have reached Los Angeles, while the MMI 4 alerts would have reached San Diego (Figure 6B). The current values of the pause parameters of 5 s and 100 km were chosen to prevent this type of over alerting in moderate earthquakes without preventing usable warning times at epicentral distances beyond the pause radius during large events. This feature has reduced over-alerting for moderate earthquakes that results from the small amount of data used in the initial earthquake location and magnitude estimates.

2.2 Algorithm association

In most moderate earthquakes, the SA receives updated location and magnitude estimates from both EPIC and FinDer during the pause time, e.g. the first 5 s after publishing the first ShakeAlert Message. A key improvement of V3 is the criteria used for associating the two algorithms as the same event. In V2, an EPIC event and a FinDer event would be associated if their locations were within 100 km and their origin times were within 30 s [Kohler et al., 2020]. While this worked well in general, there were problems with 'split events', often in regions of sparse station coverage [Lux et al., 2024] or with multiple earthquakes that were close in time [Böse et al., 2023b]. To overcome this, the association algorithm was modified starting in V.2.2.0 to be based on matching the station set that was part of each algorithm's initial detection (see Supplementary Table 1). Currently, algorithms report either the eight (EPIC) or six (FinDer) stations with the highest amplitude signals (PGA and PGV). The two events are associated together if they each have at least 3 stations within 50 km of a station used by the other algorithm and peak ground motion times within 60 s of the times from a station used by the other algorithm. In offline testing, this modification improved the EPIC and FinDer associations for earthquakes outside the station network, such as in northern Mexico or offshore northern California where the distance between the FinDer line source and the EPIC point source locations can be large. Lastly, the GFAST-PGD algorithm is initiated by listening to the SA messages and does not contribute its magnitude estimate unless there is a SA event with a magnitude estimate of 6.0 or larger and GFAST-PGD's magnitude estimate is at least 7.0. Thus, GFAST-PGD is always associated with an existing event that was initiated by one of EPIC or FinDer.

2.3 Ground motion prediction

The eqInfo2GM module takes the point and line source parameters from the SA and produces estimates of the median PGA, PGV, and MMI measures of free-field ground shaking at a given distance [Thakoor et al., 2019]. In V3, the PGA and PGV values are calculated using the ground-motion-prediction equations (GMPEs) of the Next Generation Attenuation (NGA) model from Boore and Atkinson [2008], Chiou and Youngs [2008], and Atkinson and Boore [2011]. These are converted to MMI using the ground-motion-to-intensity conversion equations (GMICEs) of Worden et al. [2012] as implemented in the USGS ShakeMap product [Wald et al., 2022]. ShakeAlert is also testing the average of the more recent Next Generation Attenuation-West (NGAW2) models [Bozorgnia et al., 2014] but they are not in production yet [Saunders et al., 2024]. The combination of the GMPEs and GMICE lead to a growth of the contour product radius with distance (Figure S3) that typically corresponds to a growth in alert area with time during the rupture of a large earthquake (Figure 7). The MMI 3 contour product is currently defined as the distance at which the median expected shaking is MMI 2.5 using the above GMPEs and GMICE such that it encloses the region where shaking is expected to be MMI 3 and above [Given et al., 2018]. Similar definitions are used for the higher MMI contour products (e.g MMI 4 contour is the distance to median MMI 3.5, etc), see Saunders et al., [2024] for a discussion of the grid and contour calculations. Recorded ground motions vary significantly over short distances due to local site and other effects. ShakeAlert does not currently attempt to estimate those at any scale finer than the 0.2 by 0.2 degree (e.g. ~20 km by 20 km) map product. Thus, the predicted ground motions are treated as the median expected shaking in a zone of roughly that size [Given et al., 2018; Thakoor et al., 2019].

Several improvements to the eqInfo2GM module have been made between V2 and V3 including the switch to using lookup tables for the ground motions from a given magnitude and distance combination to increase the computational speed in large earthquakes. Secondly, there is now logic to ensure the MMI contours remain properly nested in large earthquakes. This was needed because the alert distances for different MMI contours are calculated from the epicenter if the distance is more than 4 times the line source length, but are calculated relative to the line source for higher MMI values closer in. Without this improvement the contours could intersect if the line source and epicenter estimates have significant offsets, which sometimes occurs for out-of-network earthquakes. Additionally, the DM now allows alerting if a contour/grid cell overlaps the ShakeAlert reporting area (e.g. within the boundaries of CA, OR, and WA) even if the earthquake epicenter estimate is outside that region.

Starting with v2.2.0, two new metrics were added to test key goals of ShakeAlert performance. The first, termed Metric 1 (M1), tracks the fraction of locations that observed strong shaking (MMI >=5.5) that receive at least 10 seconds of warning time in offline tests (see table 2). This metric would of course be maximized by alerting to huge distances at small magnitude levels, which would be incompatible with ShakeAlert system goals of accurate ground motion prediction across the alerting range and would be unrealistic for a public EEW system. Such a high degree of over alerting is expected to have negative consequences such as 'alert fatigue'[Ripberger et al., 2015], but those consequences in an EEW context are not yet well understood. To track and help limit over alerting, a second metric focused on the most widespread delivery mechanism Wireless Emergency Alerts (WEAs) is calculated; it is defined as the fraction of MMI 4 contour alerts that arrive before various levels (e.g. MMI_{tw}) of weak to moderate shaking. Metric 2 (M2) is less directly interpretable than Metric 1. M1 is based on injuries occurring at MMI 5.5+. (e.Peek-Asa et. al, 2000), but which value(s) of MMI_{tw} is most important for evaluating alert performance is a matter of current research. Hence Metric 2 is evaluated at a variety of MMI_{tw} levels. It very roughly characterizes the fraction of WEAs that could arrive before moderate shaking, with low M2 values indicating a high fraction of ShakeAlert-powered WEA alerts were issued to locations with peak ground motions lower than MMI_{tw}. An unskilled algorithm that simply over-alerted to a wide area would increase M1 but decrease M2. In each software test, the candidate algorithm should increase M1 in at least some key category without making M2 values significantly lower. The values of these metrics for the V.3.0.1 test are given in Table 2 for the most widely used thresholds.

Both metrics are calculated using seismograms from all available ANSS network seismic stations in the STP test suite following the definitions from Meier, [2017] and Chung et al., [2020]. This calculation is necessary because the time that MMI_{tw} is exceeded is not a simple function of epicentral distance, and the variations (e.g. ~5-20 s) can be on the order of the metrics used to evaluate ShakeAlert.

2.4 Moderate earthquakes

A key aspect of improvement in ShakeAlert V3 is the logic governing the transition from the initial EPIC point-source solution to the combined solution for moderate to large earthquakes that involves both the EPIC magnitude estimate and the FinDer finite-fault line source and associated magnitude estimate. For large earthquakes, the first magnitude estimate produced by EPIC is typically already in the moderate magnitude range between M5.5-6.0 and usually rises above M6.0 within 1-3s after the first alert (Table 2). A key aspect of the Solution Aggregator is to switch from using a weighted average for magnitudes <6.0 to using only the FinDer magnitude estimate if it is above 6.0 and larger than EPIC's magnitude estimate. The weighted average typically favors the EPIC estimate because its uncertainty decreases with the number of stations observed [Chung et al., 2019] while FinDer's magnitude uncertainty is currently fixed at 0.5 units [Böse et al., 2023a]. The V3 approach is consistent with EPIC using only the first 4 seconds of P-wave data whereas FinDer can continue to ingest new data with increased ground motions for tens of seconds during an evolving rupture. Additionally, once FinDer reaches M6.0, the line source estimate is included in the distance parameter used in the predicted ground motion calculation which results in expanded alert areas compared to a point source [Thakoor et al., 2019]. This key transition typically happens within the first few seconds after the first ShakeAlert Message is published (Table 3) and allows V3 to track the evolution of a growing rupture more rapidly.

The current SA logic is flexible enough to accommodate multiple types of behavior seen in ShakeAlert. A counter example to the expected behavior described above comes from the 2022 M6.4 Ferndale earthquake [Lux et al., 2024]. The initial ShakeAlert Message was published using the EPIC magnitude estimate, M5.6, at 7.5 s after origin time, but by 12 s the SA magnitude had reached M6.2. In this case the growth in the magnitude estimate was driven largely by EPIC which peaked at M6.7, while FinDer lagged before eventually settling at M6.2 (Figure 8). In this case, the weighted combination of the two was used for all ShakeAlert Message updates and the SA magnitude peaked at M6.6 about 17 s after origin time. Figure 8E shows the amount of waveform data available at the initial alert which is very limited, and the first few seconds after the first alert (in this case from 7-12 s after origin) is when the magnitude estimate rapidly evolved. The difference in the time history of the magnitude estimates between FinDer and EPIC in this case likely results from the depth of the rupture which began at about 18 km in the crust of the subducted Gorda plate [Shelly et al., 2024]. One of the largest ground velocities (~45 cm/s) in this earthquake was observed at a station BK.DMOR located over 43 km from the epicenter and were likely due to a combination of the earthquake's depth and rupture directivity. As a result, the location with the highest PGV received 12 s of warning time between when the MMI 3 and 4 contour products were published and when it reached MMI 5.5 shaking [Figure 8, see Lux et al., 2024 for a detailed description]. As described in Lux et al., [2024] warning times before strong shaking ranged from 0-12 s for locations that received MMI 8 shaking, 0-17 s for MMI 7 sites, and 0-23 s for MMI 6 sites. This range of outcomes is to be expected as warning times grow rapidly with the distance from the epicenter (Figure 8F). A key point in EEW is that while there may always be a late alert zone where alerts could be delivered to end-users after strong shaking has arrived, that zone will often not be spatially coincident with the zone of strongest shaking in large earthquakes. Even for moderate earthquakes like Ferndale, it is possible to provide timely and useful ShakeAlert-powered alert deliveries to the region of peak shaking.

Another key feature of V3 is that FinDer can alert without EPIC if its magnitude estimate is above M5.5 and the SA cannot associate it with a current EPIC event. This change was made to improve ShakeAlert's resilience during highly active swarms, aftershock sequences, and other complex event scenarios. Version 2 had difficulty in such scenarios as occasionally EPIC cannot properly associate triggers when multiple earthquakes happen in quick succession [Böse et al., 2023b]. The M5.5 threshold for this feature was determined based on the range of where FinDer's magnitude estimates become most reliable. It has been activated at least once in real-time for the 02/12/2024 M4.6 earthquake in El Centro California (a different event from the one in Figure 6). For this event FinDer produced a M4.9 alert at 8.2 s after origin time and the magnitude estimate eventually peaked at M5.5.

2.5 Large earthquakes

Earthquakes with magnitudes larger than 6.5 will typically require a handoff from the initial EPIC point-source parameters to the FinDer line-source model that characterizes the fault location and the continued magnitude growth. One of the best examples of this in the test suite is the 2016 M7.1 Kumamoto earthquake. Figure 9 shows the contour products at 4.9 s, 10.1 s, 21 s, and 40 s after origin time along with the FinDer line source estimates. For this earthquake the first alert is already quite large, M6.4, but it is only a point source from EPIC. M6.4 is large enough for the MMI 3 and 4 contours to be held at the pause radius. By 10 s the magnitude estimate has increased slightly to M6.5 and the contours are released to their full distances (Figure 9B, 9E). Notably at 10 s, the FinDer line-source is contributing to the shape of the MMI 6 contour. By 21 s both the MMI 5 and 6 contours are highly affected by the line source and the MMI 5 contour includes almost all the locations that eventually experience MMI 6 shaking. While the MMI 3, 4, and 5 contour products succeed at alerting almost all the locations in danger of strong shaking, the difference between the warning times from the MMI 4 and 5 contour products is significant and can be seen in the difference between panels 10C and 10F. While the MMI 4 contour product achieves 20-40 s of warning for some MMI 6 locations, the MMI 5 contour peaks at about 15-20 s. For this earthquake, only EPIC and FinDer contribute to the magnitude estimates because GFAST-PGD peaks just below the M7.0 threshold [Murray et al., 2023] at which it contributes to the current system configuration. Overall, the intense shaking from this earthquake is accurately captured by the EPIC and FinDer algorithms and the transition from a point-source to line-source based estimate occurs rapidly. While the late-alert zone is clear near the epicenter, warning times quickly increase to usable levels within about 30 km of the epicenter and are effective enough to allow useful warning times (>10 s) at most locations that experienced strong or greater shaking.

2.6 Great earthquakes

Great earthquakes are particularly challenging both scientifically and technically for an EEW system that attempts to accurately predict ground shaking. Because the rupture can last from tens of seconds in a M8 to a few minutes in a M9, the system must continue to deliver data despite any impacts on instruments and/or telemetry systems, and its algorithms must characterize the evolution of the expected shaking over those timescales. For instance, in simulations of M9 earthquakes in Cascadia, ShakeAlert must continue to update for 3 or more minutes to produce MMI 5 contour product alerts at inland cities like Seattle [McGuire et al., 2021; Thompson et al., 2023]. Moreover, most M9s occur offshore in subduction zone settings where traditional seismic data are usually not available near the fault in real time. ShakeAlert V3 addresses these challenges in part by adding the GFAST-PGD algorithm which performs very well for well-recorded great earthquakes in subduction zones as well as large onshore strike-slip ruptures [Crowell et al., 2018; Murray et al., 2023]. GFAST-PGD uses the epicenter location from the SA and contributes only a magnitude estimate based on Global Navigation Satellite Systems (GNSS) data to the SA. Currently the greatest challenge with this algorithm results from the high levels of noise, particularly outliers, in real-time processed position streams [Murray et al., 2023]. Moreover, we do not know if the FinDer or the GFAST-PGD algorithm will operate more quickly in a given large rupture due to the station distributions or which of the seismic and geodetic data streams is more prone to outages on the timescales of minutes during a great earthquake. The SA strategy described above is designed to let either algorithm expand the alerting polygons as new information arrives. In particular, the FinDer line source can continue to grow and expand the polygons even if the weighted average of the FinDer and GFAST-PGD magnitudes does not produce a sufficient change for an alert update. Additionally, the handoff between algorithms must be flexible to account for rapid increases in either GFAST-PGD or FinDer magnitude estimates without holding back the SA to wait for the other algorithm. As a result, the magnitude error estimates from FinDer and GFAST-PGD are very important in the evolution of the alerts in a great earthquake. GFAST-PGD assigns uncertainties to its magnitude estimates using an empirically derived relationship involving the magnitude estimate and time since the earthquake origin time; this approach accounts for typical GNSS time series noise which grows with time [Murray et al., 2023]. FinDer provides an estimate of the stability of the parameters of its line-source model by varying the rupture length and strike and determining the corresponding correlation and misfit values while keeping the centroid location fixed [Böse et al., 2023a]. However, a full assessment of the uncertainty is time consuming and probably not suitable for EEW applications. It was therefore decided to set the magnitude uncertainty for FinDer in ShakeAlert to a default value of 0.5 magnitude units (m.u.).

Figure 10 shows the interactions between the four algorithms for a replay of the 2003 M8.3 Tokachi Oki megathrust earthquake. This event began ~40 km offshore at a depth of ~30 km. The first alert from EPIC is significantly larger (M6.7) than for FinDer (M4.4) due to the low PGA amplitude of the first P-wave arrivals onshore (Figure 10B). Also, for offshore earthquakes, FinDer typically produces an onshore line source with a lower magnitude estimate than the true magnitude but fairly accurate ground motion predictions [Böse et al., 2023a]. The initial magnitude growth, while weighted towards EPIC, is slow from 20 to 30 s after origin time. At about 32 s the first PGD magnitude estimate is available (M7.6) which causes a rapid growth in the SA/DM magnitude estimate. While the magnitude estimate is quite large by ~40 s (Figure 10G), there is still considerable growth in the MMI 5 contour product polygon between 44 and 90 s after origin time due to the growth in the FinDer line source. The net result is that all three algorithms contribute at some point during the rupture to expanding the alert polygons. Figure 10 demonstrates that the MMI 3 and 4 contour products expand much faster than the observed shaking allowing for considerable warning times (discussed below). The expansion of the MMI 5 contour product polygon is significantly slower, but it still outpaces the expansion of the zone of strong (MMI 6) shaking at onshore locations.

3. Warning time performance

Figure 11 shows the warning time performance in offline simulations of three well recorded earthquakes, the 2019 M7.1 Ridgecrest, 2016 M7.1 Kumamoto, and 2003 M8.3 Tokachi Oki discussed before. It focuses on the warning times for sites that experienced shaking of MMI 5.5 or larger using the MMI 4 contour product. For the shallow crustal earthquakes positive warning times are possible starting about 30 km from the epicenter leading to a small number of MMI 8-9 sites having warning times of ~5-10 seconds. The dense station spacing in the Kumamoto dataset demonstrates that it is possible to get 10+ seconds of warning for the majority of MMI 7 locations and 95% of MMI 6 locations (Figure 11H). The effect of the pause radius is clearly visible for both Ridgecrest and Kumamoto (Panels 11D and 11E) and reduced warning times at large distances by the pause time (5 seconds). However, at these distances, MMI 6 is not reached until the S-wave arrives and hence the warning times still exceed ~20 seconds or more before strong shaking. For these earthquakes the magnitude estimates increase rapidly and capture much of the possible warning times at strong shaking sites by using the MMI 4 contour product. However, the performance is significantly downgraded using the MMI 5 contour product (see Figure S4). The difference results in a significant drop in the fraction of sites with 10 seconds or more of warning for M6-7 crustal earthquakes like the 2022 Ferndale or 2016 Kumamoto examples.

Figures 8, 9, 11 and S4 demonstrate that there is a considerable range in warning time outcomes even for sites at the same shaking level in a given earthquake. The expected performance of ShakeAlert® is best described as ranges of possible warning times at different shaking levels for different classes of earthquakes, such as M6-7 crustal earthquakes or M8-9 offshore megathrust earthquakes. Similarly, describing expected performance requires specifying the product being discussed as the results can be quite different (Figure S4). This range of outcomes results from many factors, but a key one is that shaking is often amplified at significant distances in certain locations by a combination of rupture directivity, path, and site effects. For instance, the 40+ seconds of warning for an MMI 9 site in the Tokachi-Oki earthquake (Figure 11I) results from a site located over 120 km from the epicenter. What is remarkable about that result is that there are numerous locations between the epicenter and the MMI 9 site that only experienced MMI 6-8 shaking, and the rupture directivity was directed away from these locations. Many of EEW's greatest successes will come from cases like these where local site amplification effects create damaging shaking at larger than average distances.

Estimating site response is a key part of ground motion modeling in seismic hazard estimation [e.g. Rathje et al., 2015 and Stewart et a., 2017] and incorporating it in ShakeAlert will help improve timely and accurate alert delivery for locations with amplified shaking that might not otherwise be alerted based on the constant site condition assumed in the contour product, or the ergodic model assumed in the map product. Most of our licensed operators use the contour product. Within ShakeAlert, the map product has always had a spatially variable value of the average shear-velocity in the upper 30 m (Vs30) used to estimate ergodic amplification effects [Boore and Atkinson, 2008; 2011; Chiou and Youngs, 2008; Thakoor et al., 2019]. The Vs30 values are a down-sampled, 0.2 by 0.2 degree, version of the model used in ShakeMap [Thompson, 2022; Heath et al., 2020]. To improve on this, V3.0.1 has implemented the nonergodic site response model for southern California developed by Parker and Baltay [2022]. The original model was developed relative to the NGAW2 Boore et al. [2014] ground motion model (GMM), but it has been calibrated for use with the NGA GMM currently used in V.3.0.1. Offline tests of the Parker and Baltay [2022] model demonstrated that it improved both alert accuracy and warning times for moderate to large earthquakes in southern California [Lin et al., 2023]. In particular, the model produces significant increases in the estimated PGV values, and hence MMI values, in areas like downtown Los Angeles [Lin et al., 2023]. The difference in predicted MMIs at a ShakeAlert grid point can be as large as about 1 MMI unit but are typically a fraction of an MMI unit. At sites with significant amplification, these differences can increase warning times by 15-20 s in some extreme cases [Lin et al., 2023]. Figure 12 shows the difference between the contour and grid products for a replay of the Ridgecrest M7.1 mainshock at the MMI_{alert}=3.5 level that is used for

WEAs. The predicted MMI values from the map product incorporating the Parker and Baltay [2022] model are generally higher than the contour as expected because the contour values are not interpolated between products (e.g. only 2.5, 3.5, and 4.5 are assigned to any location). However, some locations do produce lower shaking estimates using the site response model compared to the contour product. Overall, the map product produces more accurate estimates both in terms of the median residual and the variance of the residuals. The largest differences between the contour and map product at a given location are in the 1-1.5 MMI unit range (Figure 12C). These are large enough in certain cases to imply different alerting areas between ShakeAlert delivery mechanisms using one product versus the other. The amplified shaking estimates produce earlier alerts for some combinations of location and MMI_{alert} which can increase warning times by as much as 10 seconds. Additionally, there are some regions where warning times can decrease relative to the contour product. The site response model has its largest impact in the highly populated Los Angeles basin and hence could lead to improved alert performance for many users.

3.2 Summary of warning time results for Japan and the West Coast

The performance seen in Figure 11 are some of the best cases for each of the three subsets of the test suite because they are among the largest earthquakes in each and hence have strong shaking spread out over large areas enabling the potential for large warning times. Collectively the test suites contain 238, 704, and 948 seismic records of strong shaking for the West Coast, Japan crustal, and Japan subduction respectively. These datasets allow us to average over the considerable variability between earthquakes and at a given distance range. The overall warning time performance for the MMI 3, 4, and 5 contour products is shown in Figure 13 and similarly for the grid product at the same MMI_{alert} levels in Figure S5. In general, both the MMI 3 and 4 contour products expand quickly enough to realize most of the possible warning time and hence there is little difference in their curves despite the MMI 3 product typically covering about a factor of 3-5 larger area in any given alert (after the pause time has passed). In contrast, the difference between the MMI 4 and 5 contour products is quite substantial in the regions where potentially damaging shaking occurs (Figures 9, 11, S4, 13). This is particularly significant for onshore crustal earthquakes as the number of locations where it is possible to achieve enough warning time for DCHO (after including data and alert delivery latencies) is typically less than 50% of strong-shaking locations. For instance, assuming a total of 5 seconds of latency for data and alert delivery, leads to only about 25% of strong shaking sites getting >10 s of warning from the MMI 5 contour product even in M6-7 crustal earthquakes (Figure 13B). The large discrepancy between the MMI 4 and 5 contour products reflects the time required for the rupture and hence the magnitude estimate to grow. Figure S5 shows a comparison of how the warning times increase with distance for two large crustal earthquakes in Japan. This magnitude of difference was seen in real time results for the M6.4 Ferndale earthquake (Figure 8) where the warning times without delivery latencies at MMI 7 sites ranged from 0-17 s for the MMI 4 contour product but only 0-11 s for the MMI 5 contour product. This significant difference in warning times has been clear in both ShakeAlert real time and offline simulations [Chung et al., 2020; McGuire et al., 2021; Thompson et al., 2023; Lux et al., 2024] and poses a challenge for implementing alerting via delivery mechanisms that have reasons to avoid alerting for mild shaking.

The significant difference in performance for the MMI 4 and 5 contour products results from the relationship between the physical and algorithmic limits on how quickly magnitude estimates can increase and the distance range where successful warning times are possible for strong shaking. Figure 14 shows the times at which MMI 6+ shaking began in the West Coast and

Japan crustal test suites compared to the times that MMI 4 and 5 contour product shaking estimates were issued. Within the late alert zone (roughly 0-30 km epicentral distance, see Figure 11G and H) there is considerable overlap between the MMI 4 and 5 contours, but most do not provide the 5-15 s required for DCHO after accounting for data telemetry and alert delivery latencies (~2-10 s). In the zone between about 30 km and 100 km the fraction of MMI 6+ locations where ShakeAlert can potentially achieve its primary goal increases, and these locations dominate the various warning time curves in Figure 13A and 13B for times larger than 10 seconds. The MMI 4 contour estimates are significantly faster for many earthquake-location pairs within this distance range which leads to most of the overall improved performance seen in Figures 10C vs 10F and in Figures 14A and 14B. Roughly 70% of MMI 8-10 sites in the West Coast and Japan Crustal test suites are within the late alert zone, while about 50% of MMI 6-7 sites are between the late alert zone and the pause radius (Figure S6). The MMI 4 contour product produces the warning time results in Figures 14A and 14B because it is defined as reaching that 100 km pause radius at the magnitude 5.6 level, which is often exceeded in the first alert for large earthquakes (Table 3). In contrast, the MMI 5 contour product currently does not reach the 100 km radius until about M6.7 (Figure S6), which typically takes an additional 5-10 seconds of additional updates after the first alert in large earthquakes. This relative ineffectiveness at achieving ShakeAlert's primary goal of the MMI 5 contour product compared to the MMI 4 product has been borne out by the overall performance in offline tests (Figure 13A and B) and real-time results [Chung et al., 2020, Lux et al., 2024] for M6-7 crustal earthquakes.

4. Ground motion accuracy

ShakeAlert V3 uses the NGA GMPEs (e.g. Boore and Atkinson [2008], and Atkinson and Boore [2011] in California and Chiou and Youngs [2008] in the Pacific Northwest) and the Worden et al. [2012] GMICE to produce its median shaking estimates which, when combined with the ShakeAlert source estimates, overall are close to unbiased albeit with considerable scatter. Figure 15 shows the range of maximum observed MMI values from the map product compared to the MMI values computed from the observed seismograms for the three components of the test suite. Panels A, B, and C show the performance in 1 MMI unit bins, while Panels D, E, and F show the aggregate across all records. There are some differences between the three datasets but all are close to zero median with a 1 MMI unit standard deviation across a wide range from MMI 2 to 7.

When the NGA GMPEs were designed there were not a lot of data from large earthquakes at significant distances (>200 km) available [Chiou et al., 2008; Power et al. 2008] and hence these GMPEs are expected to be less accurate beyond that 200 km range. It is very possible that ShakeAlert will switch to using the NGAW2 GMPEs or make other future improvements to allow more accurate GM predictions at large distances [Saunders et al., 2024]. However, the combination of the current level of source parameter accuracy with the NGA GMPEs produces estimates with only very small biases in the key alerting range from MMI 2.5 to 4.5 (Figure 15 A, B, C). In fact, Figure 15 demonstrates that ShakeAlert has achieved its original design goal of accurate alerting between MMI 2 and 8 [Given et al., 2014] to a large degree. It should be noted that Figure 15 does not consider timeliness and simply depicts the largest predicted value at a given location regardless of its timeliness. The standard deviations of the residuals for all 3 test suites are about 0.75 MMI units despite the GMPEs not being tailored for Japan and the lack of implementation of site correction models outside of Southern California.

5. Discussion

Accurate depiction of the range of results that an EEW system can provide is key for encouraging adoption and effective use of this technology. Overly optimistic information on warning times or ground-motion accuracy can encourage protective actions that are inappropriate and potentially dangerous. For instance, evacuation is recommended for some EEW systems but discouraged in other countries based on expected warning times and the specific tectonic environment of the system [McBride et al., 2022]. Similarly, the setting of EEW alert delivery thresholds can use levels that are not likely to result in enough warning time for some protective or automated actions to complete. Overly pessimistic descriptions of the EEW problem can potentially endanger people by discouraging investment in the fastest delivery technologies (e.g. machine-to-machine internet-based systems). The tension between ground-motion accuracy and timeliness will always be a key part of EEW, and while Figure 15 indicates ShakeAlert has made considerable progress on accuracy, only certain products currently provide sufficient warning times for protective actions in crustal earthquakes (Figures 9, 11, 13).

Our most important result is that ShakeAlert can provide usable warning times (10 s or more) via two of its most widely deployed products (the MMI 4 contour product for Wireless Emergency Alerts and MMI 3 contour product for cellphone applications) for most sites that experience strong shaking in M6-7 crustal earthquakes (Figure 13B) and M7-9 offshore megathrust earthquake (Figure 13C). Crustal earthquakes are challenging for EEW, and there will almost always be a late alert zone near the epicenter where usable warnings are not possible. Many of the MMI 8-10 sites will be within the late alert zone for M6-7 earthquakes (Figure S6) but a fraction are beyond it, particularly for M7 earthquakes like the 2016 Kumamoto M7 (Figure 11H). Indeed, ShakeAlert has already achieved maximum warning times of up to 17s for an MMI

7 site in real-time for a relatively moderate magnitude M6.4 earthquake [Lux et al., 2024]. As earthquakes grow larger and/or are offshore, the ability to provide warning times of a few tens of seconds at MMI 8-10 sites becomes feasible (Figures 11, 13). Alert delivery latencies vary widely and reduce warning times compared to the values quoted here, but the technology is rapidly evolving. Many delivery mechanisms connected via the internet (e.g. cell phones connected to WiFi) will deliver the alert less than 1 second after it is issued to a large fraction, and to large total numbers of their users [McGuire and de Groot, 2020], which will enable considerable successes in future large earthquakes.

The results for the MMI 5 contour product are more complex. It is possible to achieve warning times greater than 10 s for some locations of strong or greater shaking using the MMI 5 contour product (Figures 9, 11, S4), particularly for larger M7-8 earthquakes. However, the overall performance is strongly degraded compared to the MMI 4 contour product (Figures 9, 13), and at the level of M6.5 earthquakes this can prevent usable warning times [Lux et al., 2024]. Additionally, it has been shown previously that the MMI 5 contour product has difficulty providing substantial warning times in truly large subduction earthquakes in Cascadia [McGuire et al., 2021; Thompson et al., 2024] for inland locations including key cities that are far from the rupture.

ShakeAlert initially sought to provide accurate ground-motion estimates across a wide range of shaking levels (MMI 2-8) and simultaneously provide ‘seconds to minutes’ of warning time [Given et al., 2014; Burkett et al., 2014; Kohler et al., 2018; Given et al., 2018]. ShakeAlert V3 has advanced to the point where the range of outcomes is clearer. There will almost always be a late-alert zone close to the epicenter where no warning is possible before strong shaking [e.g. Chung et al., 2020], but warning times grow quickly with distance. Most ShakeAlert applications have settled into using alerting levels between MMI 2.5 and 4.5 as advised by USGS [Kohler et al., 2020] to improve warning times, but even this range may be too large to allow for success where it matters most (Figures 13 and 14). Similarly, even in truly great earthquakes that start offshore (the most optimistic scenario for EEW), like the 2003 M8.3 Tokachi-Oki earthquake, warning times can still be as short as 5-10 s before strong shaking and rarely exceed 50 s. Despite the inherent difficulty of alerting for locations close to the epicenter, the current algorithms are capable of providing usable warning times even for a scenario such as a shallow crustal M7 in an urban area. Figure 12 shows it is possible for ~90% of the MMI 6 and ~75% of the MMI7 sites to receive 10-40s of warning before strong shaking assuming the real-time system can approach the results from offline testing and alert delivery times are a few seconds or faster. These results illustrate the reality of successful EEW algorithms and the potential value in using EEW for public safety. However, accurate descriptions of warning times should be a range from "seconds to a few tens of seconds" to keep the focus on potentially damaging shaking and not promote the possibility of longer warning times.

ShakeAlert began live alerting with a strategy based on providing products defined as detailed and accurate ground motion predictions across a range of shaking levels. Both the ~1 MMI unit uncertainty level implied by the contour products and the higher spatial resolution and refined estimates of the grid product [Given et al., 2018] were designed to enable end users to customize alert delivery thresholds. ShakeAlert combined this range of products with the guidance that Wireless Emergency Alerts and other partners should alert for a lower level of shaking than they wanted to warn for, e.g. using the MMI 4 contour product to warn MMI 6 locations to increase warning times. This strategy has worked to some extent but also has several complications. First, it inadvertently gives delivery mechanisms a choice to only relay alerts that in many cases will not achieve ShakeAlert's primary objective, even in large crustal earthquakes (e.g. MMI 5 contour product results in Figure 13A and 13B). Second, it could potentially distort the algorithm development effort in that overestimating magnitude estimates in the early alerts can be favorable in achieving long warning times. A key secondary goal of EEW is to differentiate between large damaging earthquakes and more moderate (~M4.5-5.5) felt earthquakes that do not cause significant damage. This differentiation allows licensed operators to limit alerting by avoiding alerting in smaller earthquakes. Combining this goal with products primarily focused on ground motion accuracy produces a tension with warning times that is difficult to satisfy for locations close to the epicenter. Perhaps most importantly, this strategy created a coupling between the MMI alerting thresholds necessary to provide something close to the maximum physically possible warning times at close distances with the consequence of alerting vast areas at greater distances in large quakes. For instance, the choice to alert at the median shaking distance for MMI 4 allows a rapid expansion to ~100 km or more from the epicenter as the magnitude estimates increase from 5 to 6, but this also results in alerting vast areas that experience light shaking in M7s even though much of those areas are not in danger. There is not a need for a rapid (first few seconds after detection) alert at 200-500 km epicentral distance to achieve ShakeAlert's primary objective. There is no inherent reason why a product definition must target the same goal at all epicentral distances or for all magnitude ranges. For instance, the distance between the MMI 4 and 5 contour products is currently about 300 km vs 120 km for a M7.0 earthquake. An intermediate value would likely suffice for applications aimed at providing timely alerts for strong shaking despite the MMI 4 product being clearly preferable at small epicentral distances. As a result of these underlying conflicts that stem from its product definitions, ShakeAlert has implicitly accepted a level of overpredictions within the pause radius distance (e.g. Figures 5 and 6) to help ensure speed in large ruptures. This compromise has led to some major successes including the 2022 M6.4 Ferndale earthquake [Lux et al., 2024] with the cost of less ground motion accuracy within the pause radius.

The combination of the magnitude overestimation and the Alert Pause logic has highlighted the merits of a modified approach for ShakeAlert. Namely an emphasis on speed over accuracy close to the epicenter combined with an increased emphasis on accuracy at greater distances. This was not the original design or strategy of ShakeAlert [Given et al., 2014; Given et al., 2018]. However, it is perhaps the most natural approach to EEW. Rather than having a single objective function that applies at all locations (such as ground motion accuracy) it may be better to have different objectives as time (and alerting distance) evolves within a rupture to achieve the greatest number of successes for those in danger from strong shaking while limiting the extent to which alerts are sent to wider regions than desired by a particular application. The magnitude over-estimation in V.3.0.1 (Figure 5) effectively counteracts the problems that result from the current product definitions and hence has not been explicitly corrected for. Ideally, this strategy would be a prescribed choice to over alert in the region where users are in the most danger and success is possible (roughly epicentral distances of ~30-100 km in Figure 14). To the extent that there are downsides to over alerting, which is actively being researched by the social science research community, the two most productive ways to limit over alerting are to prioritize accuracy at longer times and larger distances and to avoid alerting for frequent small, M4-5.5, earthquakes. Future development work will likely improve the ability to differentiate M4-5.5 earthquakes from damaging earthquakes to allow some applications to limit unnecessary alerts.

The wide variety of applications and delivery mechanisms utilized by ShakeAlert means that there is no perfect combination of magnitude and MMI thresholds that satisfies all constraints. For instance, some applications will focus on alerting their users for any felt shaking while others attempt to limit alerting. Table 3 indicates that the first alerts in large earthquakes will likely be above M5.5 and therefore licensed operators that want to limit alerting while still using the MMI 3 or 4 contour products in large earthquakes could consider a magnitude threshold in this range. The vast majority of alerts with magnitude estimates below M5.5 will not be for damaging earthquakes (Figure 5). Table 3 indicates there is little downside to this approach in large earthquakes, while Figure 6 indicates it will avoid many over alerts.

ShakeAlert will have to balance accuracy in the magnitude 4.5-5.5 and MMI 3-5 range with the need for speed close to the epicenter. Figures 5, 13, 14, and 15 indicate that ShakeAlert is achieving accuracy within ~1 MMI units in most of its alerting range but not achieving its warning time objective at close-in locations of strong shaking for some key products as well as having moderate difficulty with peak magnitude estimates. Future modifications to ShakeAlert products may need to sacrifice some degree of ground motion accuracy near the epicenter to achieve improved warning times where damaging shaking occurs while still emphasizing accuracy at larger distances. In recent years, ShakeAlert has effectively moved towards this approach of emphasizing speed within the pause radius and improved accuracy beyond it. The compromise inherent in the current approach is likely unavoidable to some degree in EEW and could be more effective than encouraging all delivery mechanisms to alert at low MMI values.

The ShakeAlert algorithm base has made many key improvements over the last few years that led to the offline testing results seen in this paper. These results from offline tests with no data latency anomalies are a marked improvement over the real-time performance in the 2019 Ridgecrest earthquakes [Kohler et al., 2020; Chung et al., 2020; Böse et al., 2023a], and hopefully indicate future successes in the real-time production system are possible within the physical bounds on EEW. ShakeAlert will continue to pursue EEW research that will lead to future improvements and there are many tractable areas where performance can still be improved including: reducing the bias in the peak magnitude estimates, increasing resilience to data outages in either the seismic or geodetic data streams and averaging schemes that account for missing data, the use of fault specific templates in FinDer, incorporating additional site response models, further incorporation of detailed understanding of algorithm behavior to improve the SA, reductions in noise in processed GNSS displacement time series, reduced delivery latencies, and grid product optimization (size vs computation). All of these are currently being investigated. There are also possibilities related to how ShakeAlert's products are defined, including: new product definitions aimed at damaging shaking rather than median shaking, a closer connection in both product definitions and evaluation metrics to ground motion parameters that matter for injuries such as PGV and spectral accelerations at periods relevant for building damage rather than for felt shaking (e.g. PGA), and probabilistic formulations beyond the median. Lastly, there are larger scale modifications to the system that could have first order impacts. For instance, in offshore earthquakes, the first alert time is often 10-20 s after origin time (See Figure 10) rather than 4-8 s onshore [Lux et al., 2024]. The addition of offshore instrumentation could close this gap and perhaps the most promising avenue is the use of fiber optic sensing on submarine cables [Lior et al., 2023; Yin et al., 2023]. While there are challenges to operationalizing that technology in an EEW system, it is an area of rapid progress, and traditional seismic sensors telemetered by submarine cables are already part of warning systems in Japan, Taiwan, and Canada [Aoi et al., 2020; Wu et al., 2021; Schlesinger et al., 2021]. In short, there remain many avenues to continue the improvement of both the timeliness and accuracy of the ShakeAlert system.

6. Conclusions

ShakeAlert communication, education and outreach resources and our Wireless Emergency Alert messages use Drop, Cover, and Hold On as the primary protective action to take when receiving an EEW alert within the U.S. to reduce injuries [Jones and Benthien, 2011; Porter and Jones, 2018; McBride et al., 2022]. The range of likely warning times found in this study support that conclusion. Even in large M7-8 earthquakes, users should only expect seconds to a few tens of seconds of warning before strong shaking even in the best cases, and hence DCHO remains the preferred action for most users within the U.S.. Given the scale of likely warning times, education and training of what to do when receiving an alert will continue to be key to increasing EEW's effectiveness. ShakeAlert will continue to expand its set of licensed operators that deliver alerts and systems that use internet-based mechanisms may grow in importance, compared to purely cell network alerts, due to their faster delivery times. Even a few seconds improvement in delivery times can be important, and we expect the fraction of alerts delivered via internet either for public cell phone alerting (e.g. WiFi) or machine-to-machine applications will continue to grow and improve ShakeAlert's effectiveness.

ShakeAlert has progressed greatly over the last few years towards improving its performance in large earthquakes and the accuracy of its original set of products: event messages with location and magnitude estimates as well as median shaking estimates described either as a contour message or a map message. ShakeAlert is built upon a strategy that allows licensed operators to choose different combinations of expected ground motion parameters and earthquake magnitude to decide what actions to initiate, within USGS established thresholds. While products with alerting levels from MMI 2.5 to 4.5 can have considerable success in key cases (Figure 13), they present complex choices by coupling warning time success in locations of strong shaking with alerting to large distances where shaking is mild, (e.g. the MMI 3 or 4 contour products).

Many delivery mechanisms have clear reasons for limiting alerts to serve their end-users well or satisfy legal constraints. Our study shows that there is room to raise the magnitude thresholds for taking action up to about M5.5 without adversely affecting performance in large earthquakes (Table 2) and therefore this may be one way to limit alerting in some applications. The choice of ground motion alerting threshold is more complex owing to the significant drop-off in performance between the MMI 4 to 5 contour products as well as the large distances to which alerts can expand. As the EEW community develops a better understanding of what types of over alerting it is trying to avoid, it is possible that ShakeAlert will add additional products with definitions that are designed to merge those constraints with strategies aimed at its primary goal of maximizing warning times in regions of damaging shaking. However, the products that are already widely used, such as the MMI 3 and 4 contour products can provide enough warning time before strong shaking in moderate (M6) to great (M8-9) earthquakes to enable a range of protective actions.

Data and Resources

The Supplementary Information contains tables that describe the evolution of the ShakeAlert software (supplementary table 1) and the test suite (supplementary table 2). It also contains supplementary figures S1-S6.

ShakeAlert code is governed by an intellectual property agreement among the contributing authors. The ShakeAlert code is not publicly released.

The Apache ActiveMQ software is available from https://activemq.apache.org. Last accessed Nov 21, 2024.

The Apache Kafka software is available from https://kafka.apache.org. Last Accessed Nov 21, 2024.

ShakeAlert event summaries and parameters are available from the U.S. Geological Survey via the contributor code "EW" through the National Earthquake Information Center's catalog search tools https://earthquake.usgs.gov/earthquakes/search/. Last accessed March, 2024.

ShakeAlert website: https://www.shakealert.org. Last accessed March, 2024.

All seismogram data used in this study are archived at either the Southern California Earthquake Data Center [SCEDC, 2013], the Northern California Earthquake Data Center [NCEDC, 2014], the Japanese National Research Institute for Earth Science and Disaster Resilience [NIED, 2019] or the EarthScope Consortium Web Services (*https://service.iris.edu/*).

Data for the offline testing was obtained from the following seismic networks: (1) the AZ (ANZA; UC San Diego, 1982); (2) the BC (RESNOM; Centro de Investigación Científica y de Educación Superior de Ensenada (CICESE), 1980); (3) the BK (BDSN; 2014, operated by the UC Berkeley Seismological Laboratory, which is archived at the Northern California Earthquake Data Center (NCEDC), doi: 10.7932/NCEDC); (4) the CC (Cascade Chain Volcano Monitoring; Cascades Volcano Observatory, 2001); (5) the CE (CSMIP; California Division of Mines and Geology, 1972); (6) the CI (SCSN; California Institute of Technology and United States Geological Survey Pasadena, 1926); the CN (CNSN; Natural Resources Canada, 1975); the IU (GSN; Albuquerque Seismological Laboratory/USGS, 2014); the NN (Nevada Seismic Network; University of Nevada, Reno, 1972); the NP (NSMP; United States Geological Survey, 1931); the NV (NEPTUNE; Ocean Networks Canada, 2009); the UO (PNSN-UO; University of Oregon, 1990); the US (USNSN; Albuquerque Seismological Laboratory/USGS, 1990); the UW (PNSN; University of Washington, 1963); and the WR (California Division of Water Resources).

Geodetic data are available through Murray et al., [2023b] and NCEDC [2022].

ComCat earthquake source information, ShakeMaps, and ShakeMap station observations were obtained from the U.S. Geological Survey (USGS, 2017, last accessed January 2024).

Acknowledgments

Any use of trade, firm, or product names is for descriptive purposes only and does not imply endorsement by the U.S. Government. This material is based upon work supported by the U.S. Geological Survey under Grant/Cooperative Agreement No. G21AC10525 to UC Berkeley, No. G21AC10532 to ETH Zurich, No. G21AC10523 to Central Washington University, No. G21AC10561 to Caltech.

Declaration of Competing Interests

The authors declare no competing interests.

References

Al Atik, A., N. Abrahamson, J. J. Bommer, F. Scherbaum, F. Cotton, and N. Kuehn (2010). The variability of ground-motion prediction models and its components, *Seismol. Res. Lett.* 81, 794–801.

Albuquerque Seismological Laboratory/USGS. (2014). *Global Seismograph Network (GSN - IRIS/USGS)* (Data set). International Federation of Digital Seismograph Networks. https://doi.org/10.7914/SN/IU

Aoi, S. *et al.* MOWLAS: NIED observation network for earthquake, tsunami and volcano. *Earth Planets Space* 72, 126 (2020).

Apple, (2023), https://support.apple.com/en-ie/guide/iphone/iph7c3d96bab/ios#:~:text=Japan%20Meteorological%20Agency.-,Go%20to%20Settings%20%3E%20Notifications.,Emergency%20Alerts%20and%20Local%20Awareness., last accessed 6/29/2024

Atkinson, G.M. and D. M. Boore (2011). Modifications to existing ground-motion prediction equations in light of new data. *Bulletin of the Seismological Society of America*, 101(3), pp.1121-1135.

BDSN (2014), Berkeley Digital Seismic Network. UC Berkeley Seismological Laboratory. Dataset. doi:10.7932/BDSN.

Boore D. M., and G. M. Atkinson (2008). Ground-Motion Prediction Equations for the Average Horizontal Component of PGA, PGV, and 5%-Damped PSA at Spectral Periods between 0.01 s and 10.0 s. Earthquake Spectra. 24(1):99-138. doi:10.1193/1.2830434.

Boore, D. M., J. P. Stewart, E. Seyhan, and G. M. Atkinson (2014). NGA-West2 equations for predicting PGA, PGV, and 5% damped PSA for shallow crustal earthquakes, Earthq. Spectra 30, 1057–1085.

Böse, M., E. Hauksson, K. Solanki, H. Kanamori, and T. H. Heaton (2009). Real-time testing of the on-site warning algorithm in southern California and its performance during the July 29 2008 Mw 5.4 Chino Hills earthquake, *Geophys. Res. Lett.* **36**, L00B03, doi: 10.1029/2008GL036366.

Böse, M., E. Hauksson, K. Solanki, H. Kanamori, Y. M. Wu, and T. H. Heaton (2009). A new trigger criterion for improved real-time performance of onsite earthquake early warning in southern California, Bull. *Seismol. Soc. Am.* **99**, no. 2A, 897–905, doi: 10.1785/0120080034.

Böse, M., T.H. Heaton, and E. Hauksson (2012). Real-time Finite Fault Rupture Detector (FinDer) for Large Earthquakes, *Geophys. J. Int.*, **191**(2), 803-812, doi: https://doi.org/10.1111/j.1365-246X.2012.05657.x.

Böse, M., C. Felizardo, and T. H. Heaton (2015). Finite-fault rupture detector (FinDer): Going real-time in California ShakeAlert warning system, *Seismol. Res. Lett.* **86**, 1692-1704, doi:10.1785/0220150154.

Böse, M., D. Smith, C. Felizardo, M.-A. Meier, T.H. Heaton and J. Clinton (2018). FinDer v. 2: Improved real-time ground-motion predictions for M2–M9 with seismic finite-source characterization. *Geophys. J. Int.* **212**(1), 725-742.

Böse, M., J. Andrews, R. Hartog, and C. Felizardo (2023a). Performance and Next Generation Development of the Finite-Fault Rupture Detector (FinDer) within the United States West Coast ShakeAlert Warning System, *Bull. Seismol. Soc. Am.* **113** (2): 648–663, doi: 10.1785/0120220183.

Böse, M., Andrews, J., O'Rourke, C., Kilb, D., Lux, A., Bunn, J. and McGuire, J. (2023b). Testing the ShakeAlert earthquake early warning system using synthesized earthquake sequences. *Seismol. Res. Lett.* **94**(1), 243-259, doi: https://doi.org/10.1785/0220220088.

Bozorgnia, Y., N.A. Abrahamson, L. A. Atik, T. D. Ancheta, G. M. Atkinson, J. W. Baker, A. Baltay, D. M. Boore, K. W. Campbell, B. S. J. Chiou, and R. Darragh, 2014. NGA-West2 research project. *Earthquake Spectra*, *30*(3), pp.973-987.

Burkett, E.R., Given, D.D. and Jones, L.M., 2014. *ShakeAlert—an earthquake early warning system for the United States west coast* (No. 2014-3083). US Geological Survey.

Butler, H., Daly, M., Doyle, A., Gillies, S., Hagen, S. and Schaub, T., 2016. *The geojson format* (No. rfc7946).

California Geological Survey. (1972). *California Strong Motion Instrumentation Program* (Data set). International Federation of Digital Seismograph Networks. https://doi.org/10.7914/b34q-bb70

California Institute of Technology and United States Geological Survey Pasadena. (1926). *Southern California Seismic Network* (Data set). International Federation of Digital Seismograph Networks. https://doi.org/10.7914/SN/CI

Cascades Volcano Observatory/USGS. (2001). *Cascade Chain Volcano Monitoring* (Data set). International Federation of Digital Seismograph Networks. https://doi.org/10.7914/SN/CC

Centro de Investigación Científica y de Educación Superior de Ensenada (CICESE), Ensenada. (1980). *Red Sísmica del Noroeste de México* (Data set). International Federation of Digital Seismograph Networks. https://doi.org/10.7914/SN/BC

Chiou B.- J., and R. R. Youngs (2008). An NGA Model for the Average Horizontal Component of Peak Ground Motion and Response Spectra. Earthquake Spectra, 24 (1): 173–215. doi: https://doi.org/10.1193/1.2894832.

Chiou B, Darragh R, Gregor N, Silva W. NGA Project Strong-Motion Database. *Earthquake Spectra*. 2008;24(1):23-44. doi:10.1193/1.2894831

Chung, A.I., Meier, M.A., Andrews, J., Böse, M., Crowell, B.W., McGuire, J.J. and Smith, D.E. (2020). ShakeAlert earthquake early warning system performance during the 2019 Ridgecrest earthquake sequence. *Bull. Seismol. Soc. Am.* **110**(4), 1904-1923.

Cochran, E.S., M.D. Kohler, D.D. Given, S. Guiwits, J. Andrews, M.-A. Meier, M. Ahmad, I. Henson, R. Hartog, and D. Smith (2018). Earthquake Early Warning shakeAlert System: Testing and Certification Platform. *Seismol. Res. Lett*. **89**(1), 108-117, doi: 10.1785/0220170138

Crowell, B. W. (2024). Chapter 6: Earthquake and tsunami early warning with global navigation satellite system data. In GNSS Monitoring of the Terrestrial Environment, edited by Yosuke Aoki and Corne Kreemer, Elsevier.

Crowell, B. W., D. A. Schmidt, P. Bodin, J. E. Vidale, J. Gomberg, J. R. Hartog, V. C. Kress, T. I. Melbourne, M. Santillan, S. E. Minson (2016). Demonstration of the Cascadia G-FAST geodetic earthquake early warning system for the Nisqually, Washington, earthquake, *Seismol. Res. Lett.* **87** 930–943, doi: 10.1785/0220150255.

Crowell, B.W., Melgar, D. and Geng, J., 2018. Hypothetical real-time GNSS modeling of the 2016 M w 7.8 Kaikōura earthquake: Perspectives from ground motion and tsunami inundation prediction. *Bulletin of the Seismological Society of America*, *108*(3B), pp.1736-1745.

Dossot, D., 2014. *RabbitMQ essentials*. Packt Publishing Ltd.

Federal Communications Commission (2015). Wireless Emergency Alerts (WEA) Retrieved from https://www.fcc.gov/consumers/guides/wireless-emergency-alerts-wea.

FEMA (2024). IPAWS delivery systems retrieved from from: https://www.fema.gov/emergency-managers/practitioners/integrated-public-alert-warning-system

Friberg, P., S. Lisowski, I. Dricker, and S. Hellman (2010). Earthworm in the 21st century, Geophys. Res. Abstr. 12, Abstract, EGU 2010–12654.

Given, D.D., Cochran, E.S., Heaton, T., Hauksson, E., Allen, R., Hellweg, P., Vidale, J., and Bodin, P., 2014, Technical implementation plan for the ShakeAlert production system—An

Earthquake Early Warning system for the West Coast of the United States: U.S. Geological Survey Open-File Report 2014–1097, 25 p., *https://dx.doi.org/10.3133/ofr20141097*.

Given, D.D., Allen, R.M., Baltay, A.S., Bodin, P., Cochran, E.S., Creager, K., de Groot, R.M., Gee, L.S., Hauksson, E., Heaton, T.H. and Hellweg, M. (2018). Revised technical implementation plan for the ShakeAlert system—An earthquake early warning system for the West Coast of the United States (No. 2018-1155). US Geological Survey.

Hartog, R. J., P. A. Friberg,, V.C. Kress, P. Bodin, and R. Bhadha, (2020). Open-source ANSS quake monitoring system software. *Seismological Research Letters*, *91*(2A), pp.677-686.

Heath, D.C., D. J. Wald, C. B. Worden, E.M. Thompson, and G. M. Smoczyk, 2020. A global hybrid VS 30 map with a topographic slope–based default and regional map insets. *Earthquake Spectra*, *36*(3), pp.1570-1584.

Hodgkinson, K.M., D. J. Mencin, K. Feaux, C. Sievers, and G.S. Mattioli, (2020). Evaluation of earthquake magnitude estimation and event detection thresholds for real-time GNSS networks: Examples from recent events captured by the network of the Americas. *Seismological Research Letters*, *91*(3), pp.1628-1645.

Kohler, M.D., E.S. Cochran, D. Given, S. Guiwits, D. Neuhauser, I. Henson, R. Hartog, P. Bodin, V. Kress, S. Thompson, Cl. Felizardo, J. Brody, R. Bhadha, and S. Schwarz (2018).

Earthquake Early Warning ShakeAlert System: West Coast Wide Production Prototype. *Seismol. Res. Lett*., **89**, 99-107, doi: 10.1785/0220170140.

Kohler, M.D., D.E. Smith, J. Andrews, A.I. Chung, R. Hartog, I. Henson, D.D. Given, R. de Groot, and S. Guiwits (2020). Earthquake Early Warning ShakeAlert 2.0: Public Rollout. *Seismol. Res. Lett.*, **91**, 1763-1775, doi: 10.1785/0220190245.

Lin, R., G. A. Parker, J. J. McGuire, and A. S. Baltay (2023). Applications of Nonergodic Site Response Models to ShakeAlert Case Studies in the Los Angeles Area, Bull. Seismol. Soc. Am. 113, 1324–1343, doi: 10.1785/0120220145.

Lior, I., D. Rivet, J.P. Ampuero, A. Sladen, S. Barrientos, R. Sánchez-Olavarría, G. A. Villarroel Opazo, and J. A. Bustamante Prado, (2023). Magnitude estimation and ground motion prediction to harness fiber optic distributed acoustic sensing for earthquake early warning. *Scientific Reports*, *13*(1), p.424.

Lux, A. I., D. Smith, M. Böse, J. J. McGuire, J. K. Saunders, M. Huynh, I. Stubailo, J. Andrews, G. Lotto, B. Crowell, S. Crane, R. M. Allen, D. Given, R. Hartog, T. Heaton, A. Husker, J. Marty, L. O’Driscoll, H. Tobin, D. Toomey, 2024, Performance of the ShakeAlert Earthquake Early Warning System: 2019-2023, 2024, *Bulletin of the Seismological Society of America*, in press.

McBride, S.K., H. Smith, M. Morgoch, D. Sumy, M. Jenkins, L. Peek, A. Bostrom, D. Baldwin, E. Redd, R. de Groot, and J. Becker, 2022. Evidence-based guidelines for protective actions and earthquake early warning systems. *Geophysics*, *87*(1), pp.WA77-WA102.

McGuire, J. J., and R. M. de Groot, What if the ShakeAlert Earthquake Early Warning System had been operating during the M6.7 1994 Northridge Earthquake (2020), https://www.shakealert.org/wp-content/uploads/2024/01/Northridge_ShakeAlertOrg_FINAL_a_20240116.pdf

McGuire, J.J., Smith, D.E., Frankel, A.D., Wirth, E.A., McBride, S.K., and de Groot, R.M. (2021). Expected warning times from the ShakeAlert earthquake early warning system for earthquakes in the Pacific Northwest (ver. 1.1, March 24, 2021): U.S. Geological Survey Open-File Report 2021–1026, 37 p., https://doi.org/10.3133/ofr20211026.

Meier, M.-A. (2017). How "good" are real-time ground motion predictions from earthquake early warning systems? J. Geophys. Res. 122, no. 7, 5561–5577.

Meier, M.A., Kodera, Y., Böse, M., Chung, A., Hoshiba, M., Cochran, E., Minson, S., Hauksson, E. and Heaton, T., 2020. How often can earthquake early warning systems alert sites with high-intensity ground motion?, *Journal of Geophysical Research: Solid Earth*, *125*(2), p.e2019JB017718.

Melbourne, T. I., W. M. Szeliga, V. Marcelo Santillan, and C. W. Scrivner (2021). Global Navigational Satellite System Seismic Monitoring, Bull. Seismol. Soc. Am. 111, 1248–1262, doi: 10.1785/0120200356.

Melgar, D., T. I. Melbourne, B. W. Crowell, J. Geng, W. Szeliga, C. Scrivner, M. Santillan, and D. E. Goldberg (2019). Real-Time high-rate GNSS displacements: Performance demonstration during the 2019 Ridgecrest, California, earthquakes, *Seismol. Res. Lett.* **91** 1943–1951, doi: 10.1785/0220190223.

Minson, S.E., Meier, M.A., Baltay, A.S., Hanks, T.C. and Cochran, E.S., 2018. The limits of earthquake early warning: Timeliness of ground motion estimates. *Science advances*, *4*(3), p.eaaq0504.

Murray, J.R., B. W. Crowell, M. H. Murray, C. W. Ulberg, J. J. McGuire, M. A. Aranha, M. T. Hagerty; Incorporation of Real-Time Earthquake Magnitudes Estimated via Peak Ground Displacement Scaling in the ShakeAlert Earthquake Early Warning System. *Bulletin of the Seismological Society of America,* 2023a; 113 (3): 1286–1310. doi: https://doi.org/10.1785/0120220181

Murray, J. R. , B. W. Crowell, M. H. Murray, C. W. Ulberg, J. J. McGuire, M. Aranha, and M. Hagerty (2023). Input for assessing the impact of noisy data on earthquake magnitude estimates derived from peak ground displacement measured with real-time Global Navigation Satellite System data, *U.S. Geol. Surv. Data Release*, https://doi.org/10.5066/P9KXAIRR.

Natural Resources Canada (NRCAN Canada). (1975). *Canadian National Seismograph Network* (Data set). International Federation of Digital Seismograph Networks. https://doi.org/10.7914/SN/CN

NCEDC (2014). Northern California Earthquake Data Center. UC Berkeley Seismological Laboratory. Dataset. doi:10.7932/NCEDC.

NCEDC (2022). Real-time GNSS position data (https://ncedc.org/gps/rt) and metadata (https://ncedc.org/outgoing/gps/ShakeAlert/metadata/) archived at the Northern California Earthquake Data Center, doi:10.7932/NCEDC.

NIED (2019). NIED K-NET, KiK-net, National Research Institute for Earth Science and Disaster Resilience, doi:10.17598/NIED.0004.

Ocean Networks Canada. (2009). *NEPTUNE seismic stations* (Data set). International Federation of Digital Seismograph Networks. https://doi.org/10.7914/SN/NV

Patel, S.C. and R. M. Allen, 2022. The MyShake App: User experience of early warning delivery and earthquake shaking. *Seismological Society of America*, *93*(6), pp.3324-3336.

Parker, G. A., and A. S. Baltay (2022). Empirical map-based nonergodic models of site response in the greater Los Angeles area. *Bull. Seismol. Soc. Am.* 112, 1607–1629, doi: 10.1785/0120210175.

Peek-Asa, C., M.R. Ramirez, K. Shoaf, H. Seligson, and J.F. Kraus, (2000). GIS mapping of earthquake-related deaths and hospital admissions from the 1994 Northridge, California, earthquake. *Annals of Epidemiology*, *10*(1), pp.5-13.

Porter, K. and J. Jones, 2018. How many injuries can be avoided in the HayWired scenario through earthquake early warning and drop, cover, and hold on?. *Scientific Investigations Report 2017-5013-I-Q, in The HayWired Earthquake Scenario – Engineering Implications, USGS,* 429 p., https://doi.org/10.3133/sir20175013v2.

Power M, Chiou B, Abrahamson N, Bozorgnia Y, Shantz T, Roblee C. An Overview of the NGA Project. *Earthquake Spectra*. 2008;24(1):3-21. doi:10.1193/1.2894833

Rathje, E., M. Pehlivan, R. Gilbert, and A. Rodriguez-Marek, 2015. Incorporating site response into seismic hazard assessments for critical facilities: A probabilistic approach. *Perspectives on Earthquake Geotechnical Engineering: In Honour of Prof. Kenji Ishihara*, pp.93-111

Ripberger, J.T., C.L. Silva, H. C. Jenkins-Smith, D.E. Carlson, M. James, and K. G. Herron, 2015. False alarms and missed events: The impact and origins of perceived inaccuracy in tornado warning systems. Risk analysis, 35(1), pp.44-56.

Rutgers University. (2013). *Ocean Observatories Initiative* (Data set). International Federation of Digital Seismograph Networks. https://doi.org/10.7914/SN/OO

Santillan, V. M., T. I. Melbourne, W. M. Szeliga, and C. W. Scrivner (2013). A fast-convergence stream editor for real-time precise point positioning, Annual Meeting of the American Geophysical Union, San Francisco, California, 9–13 December 2013, G53B–0930.

Saunders, J.K., Baltay, A.S., Minson, S.E. and Böse, M., 2024. Uncertainty in ground-motion-to-intensity conversions significantly affects earthquake early warning alert regions. *The Seismic Record*, *4*(2), pp.121-130.

Sax, M. J., 2018; Apache Kafka, Encyclopedia of Big Data Technologies, Springer, Cham.

SCEDC (2013). Southern California Earthquake Center - Caltech [Dataset]. doi:10.7909/C3WD3xH1.

Schlesinger, A., J. Kukovica, A. Rosenberger, M. Heesemann, B. Pirenne, J. Robinson, and M. Morley, (2021) An Earthquake early warning system for Southwestern British Columbia. *Front. Earth Sci.* 9. https://doi.org/10.3389/feart.2021.684084

Shelly, D.R., Goldberg, D.E., Materna, K.Z., Skoumal, R.J., Hardebeck, J.L., Yoon, C.E., Yeck, W.L. and Earle, P.S., 2024. Subduction intraslab-interface fault interactions in the 2022 M w 6.4 Ferndale, California, earthquake sequence. *Science Advances*, *10*(10), p.eadl1226.

Smith, D., J. J. McGuire, and J. Bunn, (2024), ShakeAlert Earthquake Early Warning Testing Platform Current Developments, Fall AGU meeting, NH01-01.

Snyder, B., Bosnanac, D. and Davies, R., 2011. *ActiveMQ in action* (Vol. 47). Greenwich Conn.: Manning.

Stewart, J.P., K. Afshari, K. and C. A. Goulet, 2017. Non-ergodic site response in seismic hazard analysis. *Earthquake Spectra*, *33*(4), pp.1385-1414.

Stubailo, I., Alvarez, M., Biasi, G., Bhadha, R., and Hauksson, E. (2020). Latency of Waveform Data Delivery from the Southern California Seismic Network during the 2019 Ridgecrest Earthquake Sequence and Its Effect on ShakeAlert, *Seismol. Res. Lett.* **92**, 170–186, doi: 10.1785/0220200211

Thakoor, K., Andrews, J., Hauksson, E. and Heaton, T. (2019). From earthquake source parameters to ground-motion warnings near you: The ShakeAlert earthquake information to ground-motion (eqInfo2GM) method. *Seismol. Res. Lett.* **90**(3), 1243-1257.

Thompson, M., Hartog, J.R. and Wirth, E.A., 2003. A population-based performance evaluation of the ShakeAlert earthquake early warning system for M9 megathrust earthquakes in the Pacific Northwest, USA. Bulletin of the Seismological Society of America; doi: https://doi.org/10.1785/0120230055

Trugman, D. T., M. T. Page, S. E. Minson, and E. S. Cochran (2019). Peak ground displacement saturates exactly when expected: Implications for earthquake early warning, *J. Geophys. Res.* **124** 4642–4653, doi: 10.1029/2018JB017093.

University of Nevada, Reno. (1971). *Nevada Seismic Network* (Data set). International Federation of Digital Seismograph Networks. https://doi.org/10.7914/SN/NN

University of Oregon. (1990). *Pacific Northwest Seismic Network - University of Oregon* (Data set). International Federation of Digital Seismograph Networks. https://doi.org/10.7914/SN/UO

University of Washington. (1963). *Pacific Northwest Seismic Network - University of Washington* (Data set). International Federation of Digital Seismograph Networks. https://doi.org/10.7914/SN/UW

U.S. Geological Survey. (1931). *United States National Strong-Motion Network* (Data set). International Federation of Digital Seismograph Networks. https://doi.org/10.7914/SN/NP

U.S. Geological Survey, Earthquake Hazards Program (2017). Advanced National Seismic System (ANSS) Comprehensive Catalog of Earthquake Events and Products: Various, https://doi.org/10.5066/F7MS3QZH.

Wald, D.J., C. B., Worden, E.M. Thompson, and M. Hearne, 2022. ShakeMap operations, policies, and procedures. *Earthquake Spectra*, *38*(1), pp.756-777.

Worden, C. B., E. M. Thompson, M. Hearne, and D. J. Wald (2020). ShakeMap manual online: Technical manual, user’s guide, and software guide, U.S. Geological Survey. http://usgs.github.io/shakemap/. doi: 10.5066/F7D21VPQ.

Wu, Y.M., H. Mittal, D. Y. Chen, T. Y. Hsu. and P. Y. Lin. (2021). Earthquake early warning systems in Taiwan: Current status. *Journal of the Geological Society of India*, *97*, pp.1525-1532.

Yin, J., Soto, M.A., Ramírez, J., Kamalov, V., Zhu, W., Husker, A. and Zhan, Z., 2023. Real-Data Testing of Distributed Acoustic Sensing for Offshore Earthquake Early Warning. *The Seismic Record*, *3*(4), pp.269-277.

Author mailing addresses

Jeffrey J. McGuire, United States Geological Survey (USGS), 345 Middlefield Rd, Menlo Park, CA 94025; jmcguire@usgs.gov, https://orcid.org/0000-0001-9235-2166.

Carl W. Ulberg, Dept. of Earth and Space Sciences, University of Washington (UW), Box 351310, Seattle, WA 98195-1310; ulbergc@uw.edu, https://orcid.org/0000-0001-6198-809X.

Angela I. Lux, UC Berkeley Seismological Laboratory, 307 McCone Hall #4760, Berkeley CA 94720-4760; angie.lux@berkeley.edu, https://orcid.org/0000-0002-3767-6018

Maren Böse, Swiss Seismological Service (SED), ETH Zurich, Sonneggstr. 5, 8092, Zurich, Switzerland; maren.boese@sed.ethz.ch, https://orcid.org/0000-0003-4639-719X

Jennifer Andrews, GNS Science, PO Box 30-368, Lower Hutt 5040, New Zealand; jen.andrews@gns.cri.nz, https://orcid.org/0000-0002-5679-5565.

Deborah Smith, United States Geological Survey (USGS), 525 S Wilson Ave, Pasadena, CA 91106; deborahsmith@usgs.gov, https://orcid.org/0000-0002-8317-7762.

Brendan Crowell, Dept. of Earth and Space Sciences, University of Washington (UW), Box 351310, Seattle, WA 98195-1310; crowellb@uw.edu, https://orcid.org/0000-0001-7096-601X.

Jessica R. Murray, U.S. Geological Survey, Earthquake Science Center, P.O. Box 158 Moffett Field, CA 94035, jrmurray@usgs.gov, https://orcid.org/0000-0002-6144-1681

Ivan Henson, UC Berkeley Seismological Laboratory, 307 McCone Hall #4760, Berkeley CA 94720-4760; henson@seismo.berkeley.edu

Renate Hartog, Dept. of Earth and Space Sciences, University of Washington (UW), Box 351310, Seattle, WA 98195-1310; jrhartog@uw.edu, https://orcid.org/0000-0002-4116-7806

Claude Felizardo, California Institute of Technology (Caltech) Seismological Laboratory, 1200 E California Blvd, MS 252-21, Pasadena, CA 91125; claude@caltech.edu

Minh Huynh, United States Geological Survey (USGS), 525 S Wilson Ave, Pasadena, CA 91106; mhuynh@usgs.gov, https://orcid.org/0000-0002-5856-121X

Mario Aranha, University of California, Berkeley, Berkeley Seismological Laboratory, 205 McCone Hall, Berkeley, CA 94720-4760, maranha@berkeley.edu,

Grace Parker, U.S. Geological Survey, Earthquake Science Center, P.O. Box 158 Moffett Field, CA 94035, gparker@usgs.gov, https://orcid.org/0000-0002-9445-2571

Annemarie Baltay, U.S. Geological Survey, Earthquake Science Center, P.O. Box 158 Moffett Field, CA 94035, abaltay@usgs.gov, https://orcird.org/0000-0002-6514-852X

Mark H. Murray, U.S. Geological Survey, Earthquake Science Center, P.O. Box 158 Moffett Field, CA 94035; mhmurray@usgs.gov, https://orcid.org/0000-0003-4862-55470

Glenn Biasi, United States Geological Survey (USGS), 525 S Wilson Ave, Pasadena, CA 91106; gbiasi@usgs.gov; https://orcid.org/0000-0003-0940-5488

Steve Guiwits, United States Geological Survey (USGS), 525 S Wilson Ave, Pasadena, CA 91106; sguiwits@usgs.gov; https://orcid.org/0000-0002-6481-6231

Jessie K. Saunders, California Institute of Technology (Caltech) Seismological Laboratory, 1200 E California Blvd, MS 252-21, Pasadena, CA 91125; jsaunder@caltech.edu, https://orcid.org/0000-0001-5340-6715.

Andrew Good, California Institute of Technology (Caltech) Seismological Laboratory, 1200 E California Blvd, MS 252-21, Pasadena, CA 91125; agood@caltech.edu, https://orcid.org/0009-0002-0999-4622

V. Marcelo Santillan, Department of Geological Sciences, Central Washington University, WA 98926; marcelo@geology.cwu.edu

Craig W. Scrivner, Department of Geological Sciences, Central Washington University, WA 98926; scrivner@Geology.cwu.EDU,

Walter M. Szeliga, Department of Geological Sciences, Central Washington University, WA 98926; walter.szeliga@cwu.edu, https://orcid.org/0000-0002-9991-1204

Timothy I. Melbourne, Department of Geological Sciences, Central Washington University, WA 98926; tim@geology.cwu.edu, https://orcid.org/0000-0003-1870-3962

Victor Kress, Dept. of Earth and Space Sciences, University of Washington (UW), Box 351310, Seattle, WA 98195-1310; kress@u.washington.edu

Robert M. de Groot, United States Geological Survey (USGS), 525 S Wilson Ave, Pasadena, CA 91106; rdegroot@usgs.gov, https://orcid.org/0000-0001-9995-4207

Sara K. McBride, United States Geological Survey (USGS), 1711 Illinois Street, Golden Colorado 80401; skmcbride@usgs.gov, https://orcid.org/0000-0002-8062-6542

Douglas Given, United States Geological Survey (USGS), 525 S Wilson Ave, Pasadena, CA 91106; doug@usgs.gov, https://orcid.org/0000-0002-3277-5121

Richard M. Allen, UC Berkeley Seismological Laboratory, 307 McCone Hall #4760, Berkeley CA 94720-4760; rallen@berkeley.edu.

Thomas H. Heaton, California Institute of Technology (Caltech) Seismological Laboratory, 1200 E California Blvd, MS 252-21, Pasadena, CA 91125; heaton@caltech.edu, https://orcid.org/0000-0003-3363-2197

Allen Husker, California Institute of Technology (Caltech) Seismological Laboratory, 1200 E California Blvd, MS 252-21, Pasadena, CA 91125, ahusker@caltech.edu, https://orcid.org/0000-0003-1139-0502

Valerie Thomas, United States Geological Survey (USGS), 525 S Wilson Ave, Pasadena, CA 91106; vthomas@usgs.gov, https://orcid.org/0000-0001-6170-5563

Harold Tobin, Dept. of Earth and Space Sciences, University of Washington (UW), Box 351310, Seattle, WA 98195-1310; htobin@uw.edu, https://orcid.org/0000-0002-1447-6873

Sumant Jha, University Space Research Association (USRA), 216D, Bldg 19, NASA Ames Research Park, Mountain View, CA, sjha@usra.edu, https://orcid.org/0000-0003-0075-1712

Julian Bunn, GPS Division, California Institute of Technology, Pasadena, CA 91125; Julian.Bunn@caltech.edu; , https://orcid.org/0000-0002-3798-298X

1492

Tables

Table 1. Key features and roles of the six algorithms in ShakeAlert V3. Time ranges in the first row are approximate ranges in seconds after the initial P-wave triggers.

Algorithm	**Data Type**	**Initial Detection** (0 to ~5 s)	**Moderate Magnitude** M4.5-6 (~3-10 s)	**Large Magnitude** M6.0 -7.0 (~4-15 s)	**Great Earthquake** M 7.0-9 (>15s)
EPIC	Seismic, up to the 1st 4-5 seconds of P-wave displacement	1st alert with data at a minimum of 4 stations. Alerts alone.	magnitude weighted by duration of each P-waveform	maximum magnitude of 7.5	
FinDer	Seismic, peak acceleration values over the full event duration		Can alert alone if M>5.5 and not associated with a current EPIC event	Line Source contributes to ground motion estimates	Magnitude estimates can grow up to 9 and lengths up to 1362 km
GFAST-PGD	Geodetic, peak displacement over the			Initiated by seismic magnitude >6.0	Magnitude estimates can grow for up to 2 minutes

	full event duration				
Solution Aggregator			associates EPIC and FinDer with weighted averages for location and magnitude	uses FinDer magnitude or weighted average if EPIC is larger	If GFAST M>7.0, Magnitude is a weighted average of FinDer and GFAST
EqInfo2GM		Uses just the point source. Enforces the 100 km pause radius	Enforces pause radius until 5s after 1st alert	Uses line source and point source	Uses line source and point source
Decision Module		Throttles alerts to 1 update per second			

Table 2. Warning time metrics for the V3.0.1 STP test. M1 is the % of sites with peak shaking of MMI 5.5 or larger that received at least 10 s of warning before MMI 5.5 shaking began in offline testing. The metrics are tabulated separately for the West Coast, Japan Crustal, and Japan subduction zone portions of the test suite and separately for the contour and map products and for the MMI_{alert} levels that define the MMI 3, 4, and 5 contour products (e.g. 2.5, 3.5, and 4.5). M2 is

the percentage of sites alerted for MMI_{alert}=3.5 shaking that received 10 s of warning before various values of observed (MMI_{tw}) shaking. The M2 values correspond to the WEA delivery mechanisms that are very widely distributed and reach all cellular phones

MMI_alert	**Metric 1 West Coast contour (%)**	**Metric 1 West Coast map (%)**	**Metric 1 Japan Crust contour (%)**	**Metric 1 Japan Crust map (%)**	**Metric 1 Japan Subduction contour (%)**	**Metric 1 Japan Subduction map (%)**
2.5	34.73	32.85	55.37	55.37	92.91	93.01
3.5	32.35	28.05	55.06	54.71	88.67	89.44
4.5	13.45	7.51	41.45	41.24	69.25	69.54
MMI_tw	**Metric 2 West Coast contour (%)**	**Metric 2 West Coast map (%)**	**Metric 2 Japan Crust contour (%)**	**Metric 2 Japan Crust map (%)**	**Metric 2 Japan Subduction contour (%)**	**Metric 2 Japan Subduction map (%)**
4.0	25.35	28.22	31.63	32.36	53.34	55.55
4.5	9.30	10.55	12.37	12.66	33.45	34.75
5.0	4.86	5.34	6.33	6.45	25.45	25.99

.

1507

Table 3. First ShakeAlert magnitude and update above M6.0 in offline replays of V3 for large crustal earthquakes in well-instrumented regions, e.g. that do not include data transmission latencies. Earthquakes with an asterisk denote real-time results from the ShakeAlert system after the EPIC magnitude weighting scheme was upgraded. Times are given in seconds after the earthquake's origin time.

Earthquake	Catalog magnitude	DM First ShakeAlert Message	DM update to M6.0+
2019 Ridgecrest	7.1	M5.7 at 6 s	M6.3 at 8 s
2018 Anchorage	7.1	M4.8 at 9 s	M6.0 at 14 s
2016 Kumamoto	7.1	M5.3 at 5 s	M6.1 at 6 s
2008 Iwate	6.8	M7.1 at 6 s	M6.4 at 8 s
2000 Tottori	6.7	M5.4 at 4 s	M6.1 at 7 s
2011 Fukushima	6.6	M6.4 at 5 s	M6.2 at 8 s
2022 Ferndale*	6.4	M5.6 at 8 s	M6.2 at 12 s
2019 Ridgecrest	6.4	M5.9 at 7 s	M6.0 at 9 s
2021 Petrolia	5.7-6.2	M5.0 at 9 s	M6.0 at 13 s
2014 South Napa	6.0	M5.9 at 5 s	M6.0 at 6 s

List of Figure Captions

Figure 1. After Given et al. [2018]. Schematic view of the ShakeAlert processing algorithms. Seismic and geodetic ground motion observations are processed and then fed into three algorithms (EPIC, FinDer, and GFAST-PGD) to estimate source parameters. Those parameters are combined in the Solution Aggregator and fed to the Eqinfo2GM algorithm to produce the grid (the terms grid product and map product are used interchangeably) and contour products that estimate ground motions. Finally, the Decision Module checks to see if the alert meets publication thresholds and if so, it publishes ShakeAlert Messages with the event, contour, and map products to the alert servers. Licensed operators connect to the alert servers and subscribe to ShakeAlert Messages topics to receive these data products.

Figure 2. Summary of ShakeAlert® delivery mechanisms including the magnitude and MMI thresholds. Currently most applications use the contour product, but some have begun using the map product. Currently the intensity thresholds range from MMI 2.5 (e.g. III) to MMI 5.5 (e.g. VI) across all applications. Thus, ShakeAlert ground motion predictions are required to be relatively accurate across a wide range of shaking intensities.

Figure 3. A flow chart of the logic within the Solution Aggregator (SA) that combines the source parameters estimated by the EPIC, FinDer, and GFAST-PGD algorithms. GFAST-PGD is triggered by the seismic algorithms producing a SA magnitude estimate of 6.0 or larger and is only part of the SA evaluations when its magnitude is larger than 7.0.

Figure 4. A) Current Seismic and B) Geodetic Station distributions being utilized by the production system as of May 2024. All geodetic data flow to Central Washington University for processing. Seismic data flows to one of four processing centers at Caltech, U.S. Geological Survey, UC Berkeley or the Univ. of Washington for initial processing by algorithms that precede EPIC and FinDer in the analysis chain. See the Data Availability statement for the seismic and geodetic network descriptions and references.

Figure 5. A) Peak DM magnitude for offline replays of the West Coast test suite with V3. For earthquakes with maximum DM magnitudes between 4.5 and 6.0, the median positive bias in maximum estimated magnitude is 0.41 units. B) Peak DM magnitude for real time results for earthquakes in CA that occurred between 1/1/2022 and 2/26/2024 using various versions of the ShakeAlert system that had a maximum magnitude above M4.5. The median positive bias in the maximum estimated magnitude is 0.4 units.

Figure 6: A) Effect of the Alert Pause in the August 20^{th}, 2023, M5.1 Ojai CA earthquake. Contour products are shown for the M6.0 first alert produced by the real-time system, the fourth alert, (~6s after the first alert and M5.6), which produced the largest alert areas. The MMI 3 and 4 contours for the first alert are coincident at 100 km radius as constrained. Also shown are the contours that would have resulted from the M6.0 first alert if the pause radius was not implemented (the largest area polygons). Without the Alert Pause approach, additional MMI 3 alerts would have been sent to San Diego, Fresno, and Salinas (e.g. the region between contour 3B and 3C). Similarly, additional MMI 4 alerts would have been sent to the eastern half of Los Angeles and Santa Barbara (e.g. the region between contours 4B and 4C). B) Effect of the Alert Pause in the 2/12/2024, M4.8

El Centro earthquake. The first alert (A) was M5.8 at 5 seconds after origin time causing the MMI 3 and 4 contours (3A and 4A) to overlap at 100 km radius, after the pause time expired a M5.6 alert (B) was released. If the first alert had been released, cell phone App alerts would have gone to Los Angeles and Riverside CA (region between contours 3B and 3C). Similarly, WEAs would have gone to the suburbs of San Diego (region between contours 4A and 4C).

Figure 7. Examples of the temporal evolution of ShakeAlert contour products as the magnitude estimate grows with time during the rupture are shown from an offline replay (with no data delivery latencies included) of V3.0.1 of ShakeAlert for the 2019 Ridgecrest M7.1 earthquake. The MMI 3, 4, 5, and 6 contours are labeled and colored according to the colorbar. A-C) show the evolution of the ShakeAlert MMI estimate polygons corresponding to (A) the initial detection at 5s after the earthquake begins, (B) the moderate-large earthquake stage at 10s, and (C) the large earthquake stage at 15 s. Each map shows several of the contour product polygons for different MMI levels and the ANSS epicenter as a star. In A) the MMI 3 and 4 contour products plot on top of each other at the 100 km pause radius distance, while the MMI 5 contour product is barely visible. In B) the MMI 3, 4, and 5 contour products are visible. In C) the MMI 4, 5, 6, and 7 contour products are visible and the MMI 5-7 polygons are visibly elongated along the fault direction as estimated by the FinDer line source. The MMI 3 polygon in C) is mostly beyond the scale of the map. Currently alerts would only be delivered to users in the State of California for this earthquake even though the polygons extend into Nevada.

Figure 8: Realtime results from the 2022 M6.4 Ferndale earthquake. A-C) Maps of the first ShakeAlert Contour Message, the 6th update, and the 10th update respectively. The MMI 3, 4,

and 5 contour products are shown with the MMI color scale. In panels A and B, the MMI 3 and 4 contours are coincident due to the pause radius. In Panel C, the MMI 3 and 4 contours are beyond the edge of the map. The EPIC epicenter and FinDer line source estimates are shown with red stars and lines respectively. D) Magnitude estimates as a function of time from the production system for the EPIC, FinDer, and DM algorithms. E) Examples of horizontal component seismograms for high amplitude stations. Each station shows the N-S component of ground velocity and is labeled with its station code and peak velocity. F) Map of the epicenter (star) and station locations (diamonds). Light gray lines denote major roadways. Each station is labeled with its peak MMI value and warning time (e.g. 7:17s means peak MMI of 7 and 17 s maximum warning time without delivery latency). The color scale of the diamonds denotes the warning time for the MMI 4 contour product before MMI 5.5 shaking began. Contours show regions of different MMI levels and are colored according to the usual ShakeMap color table for MMI.

Figure 9. Progression of the MMI 4, 5, and 6 contour products during an offline simulation of the 2016 M7.1 Kumamoto earthquake (star denotes the ANSS epicenter estimate). Panels A, B, and C show warning times before MMI 6 shaking from the MMI 4 contour product at individual stations (diamonds). Only the seismic stations that had peak shaking of MMI 6 or higher are shown. The warning time color scale is the same in all panels. Each panel shows the MMI 4 (light blue), MMI 5 (green) and MMI 6 (yellow) contour products. Each panel is labeled with the seconds after origin time that the DM published the ShakeAlert Message and the associated magnitude estimate. Panels D, E, and F similarly show warning times before MMI 6 shaking from the MMI 5 contour product at individual seismic stations (diamonds). For each panel, only

the stations that have been alerted by that contour product at that time are shown. The first alert (panels A, D) is for a point source as estimated by EPIC. The later alerts at 10.1 s (panels B, E), 21 s (panel C), and 40 s (panel F) show the SA combination of EPIC and FinDer. Because these three estimates are above magnitude 6.0, they include the effect of the FinDer line source (shown as a purple line). While the MMI 5 contour product for the largest alert is sufficient to contain all the MMI 6+ sites, its slower expansion results in reduced warning times compared to those for the MMI 4 contour product (e.g. the difference between panels C and F).

Figure 10. Evolution of the magnitude estimates and alerting polygons for an offline replay of V3 for the 2003 M8.3 Tokachi-Oki megathrust subduction earthquake. A) The black, blue, magenta, and red curves show the magnitude estimate evolution from the EPIC, FinDer, GFAST, and SA/DM algorithms respectively. The gray diamonds denote the 9 alerts shown in panels B-J. B-J) Each panel shows the MMI 3, 4, and 5 contour product polygons colored according to the MMI scale and the ANSS epicenter estimate (gray star). Each panel is labeled with the number of seconds after origin time that the DM published the ShakeAlert message (e.g. T=25 is 25 seconds after origin). In panels B and C, the MMI 3 and 4 polygons are coincident due to the Alert Pause and the MMI 3 polygon is completely beyond the bounds of the map in panels H and I. Each small diamond in panels B-J denotes the location of a seismic station used in the simulation and the color denotes the peak MMI value it has reached by that alert's time since origin. The MMI 5 contour is elongated in the along-strike direction because of the FinDer line source estimate. The MMI 5 contour is also slightly offset relative to the MMI 4 contour because the line source estimate is located onshore.

Figure 11: Warning time performance of V3 in offline testing of the 2019 M7.1 Ridgecrest (panels A, D, G), 2016 M7.1 Kumamoto (panels B, E, H), and 2003 M8.3 Tokachi-Oki (panels C, F, I) earthquakes. All results are for the MMI 4 contour product from offline testing without data or delivery latencies. Panels A, B, and C show the warning times between when the MMI 4 contour product is published for that location and when that seismic station recorded MMI 5.5 (diamonds). Gray stars denote the earthquake epicenter. Panels D, E, and F show the temporal evolution of shaking at each seismic station relative to the time that location was first within the MMI 4 contour product in a ShakeAlert Message. Each station is represented as a vertical series of circles that are colored by MMI level from 2 up through the highest MMI level reached at that location. The colors are denoted by the bar adjacent to panel I. In general, warning times increase with distance from the hypocenter, but this is not monotonic because of the pause radius and the temporal evolution of magnitude estimates during the growing rupture. For some earthquakes, the warning times can be shorter at large distances (e.g. panels D and E at ~250 km) due to the temporal history of the predicted ground motions. Panels G, H, and I show cumulative distributions of warning times for groups of stations binned by their peak MMI level. All of the stations with a peak shaking between MMI 5.5 and 6.5 are shown as the yellow lines with the y-axis indicating the fraction of those stations that achieved the value of warning time along the x-axis. Only seismic stations that recorded MMI 5.5 or larger shaking are shown in the solid lines. Dashed lines for lower MMI locations are based on theoretical S-wave arrival times (see Chung et al., 2020). In general, the higher the peak shaking level, the lower the average warning time but this is not a hard rule as there is considerable overlap in the range of warning times for the different bins of peak shaking (e.g. the MMI 6, 7, 8, and 9 bins all have locations with 40 s of warning time in panel I).

Figure 12. Comparison of the contour and grid (map) product MMI predictions for the offline replay of the Ridgecrest M7.1 including the site response model in the grid product. A) Difference in peak MMI (grid - contour) at the location of seismic stations used in the simulation. B) Warning time differences between the grid product and contour products (grid - contour) using MMI_{alert}=3.5 in the Ridgecrest M7.1 mainshock. Positive differences indicate longer warning times with the grid product. C) Comparison of peak MMI values between the grid and contour products. D) and E) show differences between the predicted and observed peak MMI values using the contour and grid product respectively. The grid product has both a lower median residual and a smaller standard deviation (sigma) of residuals demonstrating its increased accuracy and precision. All predicted values in panels A, C, D, and E use the maximum shaking predicted at a site regardless of timeliness.

Figure 13: Empirical CDFs of cumulative warning times at seismic stations before strong shaking at 238, 704, and 948 MMI 6+ sites for the west coast (panel A), Japan Crustal (panel B) and Japan subduction zone (panel C). Results for the MMI 3, 4, and 5 contour products are shown as red, blue, and black curves respectively. The magnitude range is lowest for the West Coast dataset (M4.0 - 7.1) leading to shorter overall warning times than the Japan Crustal (M6.0-7.1) and Japan Subduction Zone (M7.1-9.0). Additionally, most of the subduction events begin offshore where there are no seismic stations, and thus, there are no measurements in the late alert zone for that panel.

Figure 14. Comparison of the time that strong shaking begins with the time of MMI 4 and 5 contour product alerts for the shallow crustal earthquakes in the West Coast and Japan crustal datasets.

Light blue circles denote the time that MMI 5.5 shaking began at individual seismic stations. Orange circles and dark blue diamonds denote the time that those same seismic stations were first alerted with the MMI 4 and 5 contour products respectively. Vertical lines at 30 km and 100 km epicentral distance denote the approximate location of the extent of the late alert zone and the pause radius respectively. Note the epicentral distances are with respect to the ANSS catalog epicenter (USGS 2017), not the ShakeAlert epicenter estimate that controls the calculation of the pause radius. The Y-axis is a log scale. At a given epicentral distance range, say 50-60 km, the MMI 6 exceedance time (light blue circles) can vary over about 15-20 seconds due to many factors related to how a particular earthquake ruptures. The times the MMI 4 and 5 contour product were published are from offline simulations and do not include the latencies associated with data telemetry or alert delivery which would typically add a minimum of 2 seconds to these times and can vary widely between delivery mechanisms.

Figure 15: Comparison of individual station maximum predicted and observed MMI values for the West Coast (A, D), Japan Crustal (B, E), and Japan Subduction Zone (C, F) testing datasets. All predicted values are from the map products. Panels A, B, and C show all predictions in one MMI bins and the 25 and 75th percentiles (box) as well as large outliers (red whiskers). Panels D, E, and F show individual station residuals which are dominated by MMI 2-4 levels in these datasets. Each panel gives the median and standard deviation of the residuals. These maximum predicted values encompass the performance of the entire system including the magnitude over and under estimates in individual earthquakes. In general, ShakeAlert is unbiased for all three datasets with the exception of underpredicting the highest MMI 5-7 sites in the West Coast dataset.

Figures

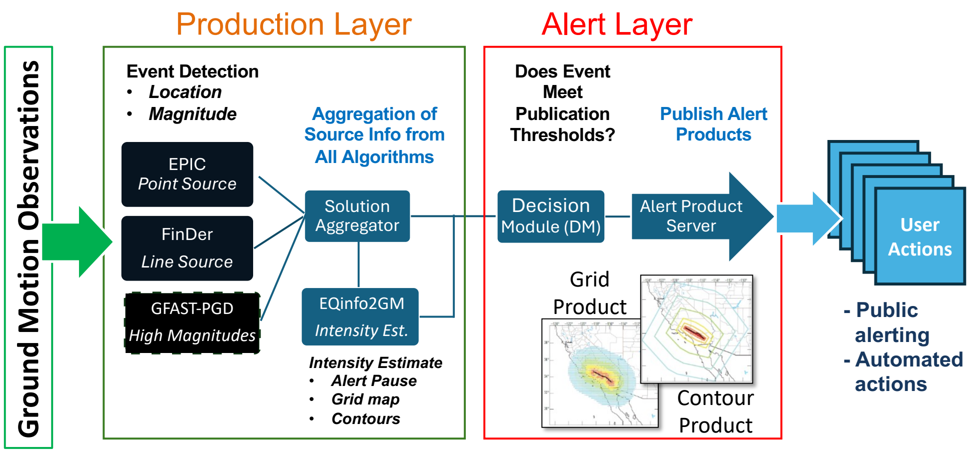

Figure 1. After Given et al. [2018]. Schematic view of the ShakeAlert processing algorithms. Seismic and geodetic ground motion observations are processed and then fed into three algorithms (EPIC, FinDer, and GFAST-PGD) to estimate source parameters. Those parameters are combined in the Solution Aggregator and fed to the Eqinfo2GM algorithm to produce the grid (the terms grid product and map product are used interchangeably) and contour products that estimate ground motions. Finally, the Decision Module checks to see if the alert meets publication thresholds and if so, it publishes ShakeAlert Messages with the event, contour, and map products to the alert servers. Licensed operators connect to the alert servers and subscribe to ShakeAlert Messages topics to receive these data products.

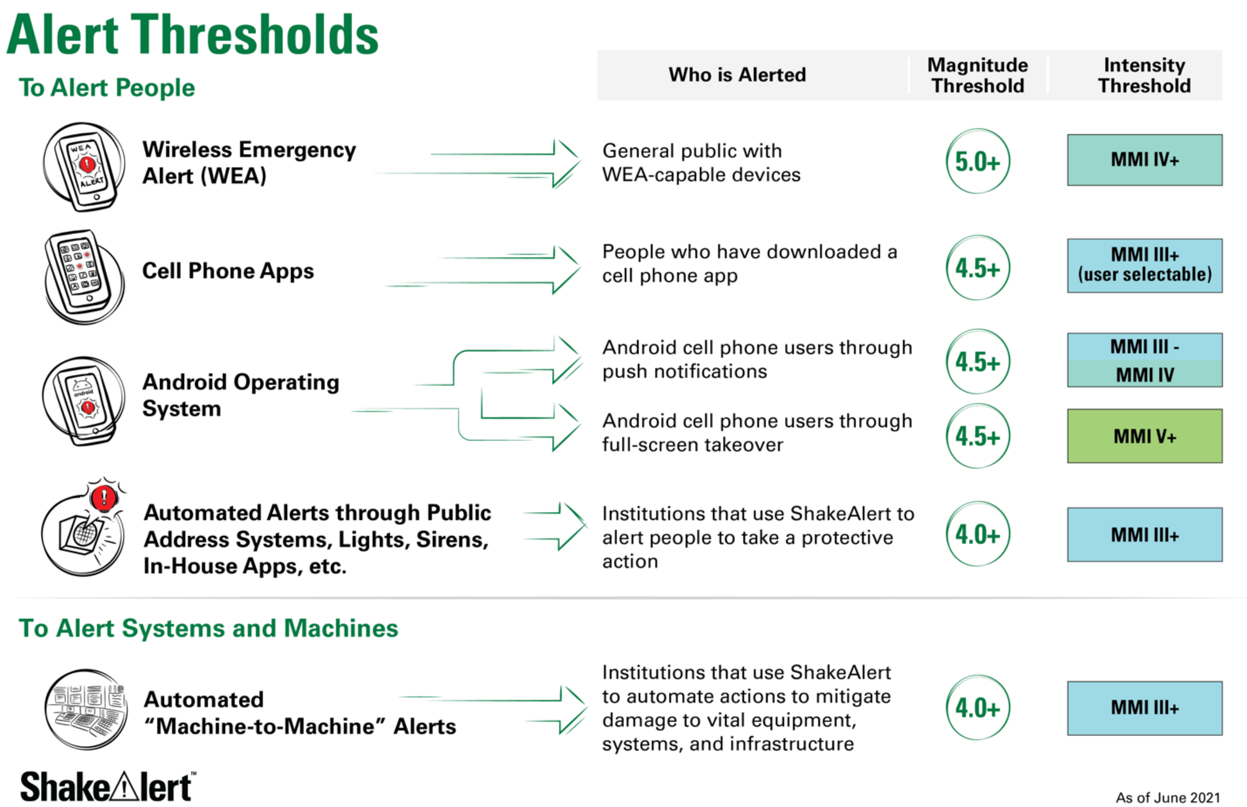

Figure 2. Summary of ShakeAlert® delivery mechanisms including the magnitude and MMI thresholds. Currently most applications use the contour product, but some have begun using the map product. Currently the intensity thresholds range from MMI 2.5 (e.g. III) to MMI 5.5 (e.g. VI) across all applications. Thus, ShakeAlert ground motion predictions are required to be relatively accurate across a wide range of shaking intensities.

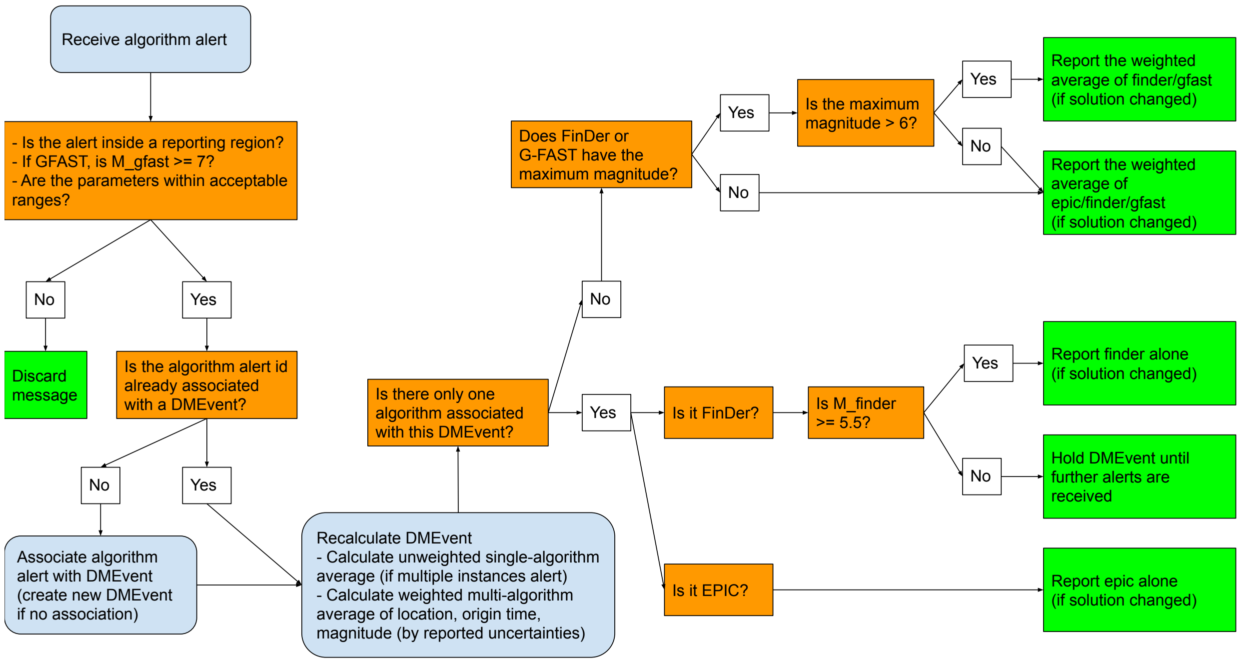

Figure 3. A flow chart of the logic within the Solution Aggregator (SA) that combines the source parameters estimated by the EPIC, FinDer, and GFAST-PGD algorithms. GFAST-PGD is triggered by the seismic algorithms producing a SA magnitude estimate of 6.0 or larger and is only part of the SA evaluations when its magnitude is larger than 7.0.

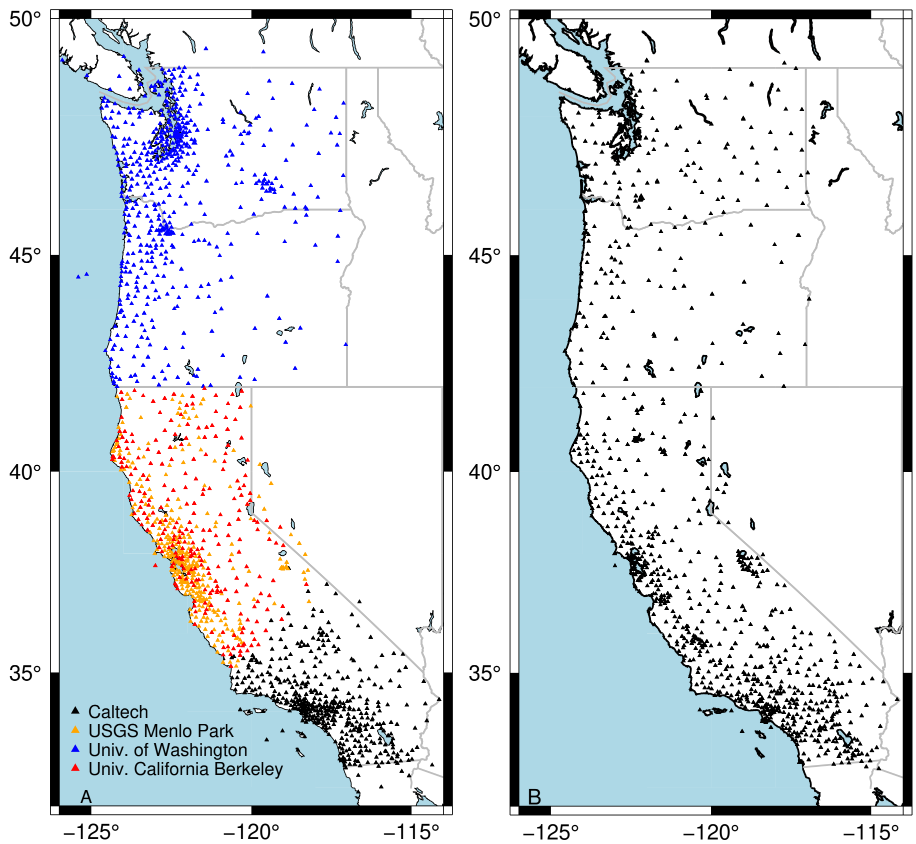

Figure 4. A) Current Seismic and B) Geodetic Station distributions being utilized by the production system. All geodetic data flow to Central Washington University for processing. Seismic data flows to one of four processing centers at Caltech, U.S Geological Survey Moffett Field, UC Berkeley or the Univ. of Washington for initial processing by algorithms that precede EPIC and FinDer in the analysis chain. See the Data Availability statement for the seismic and geodetic network descriptions and references.

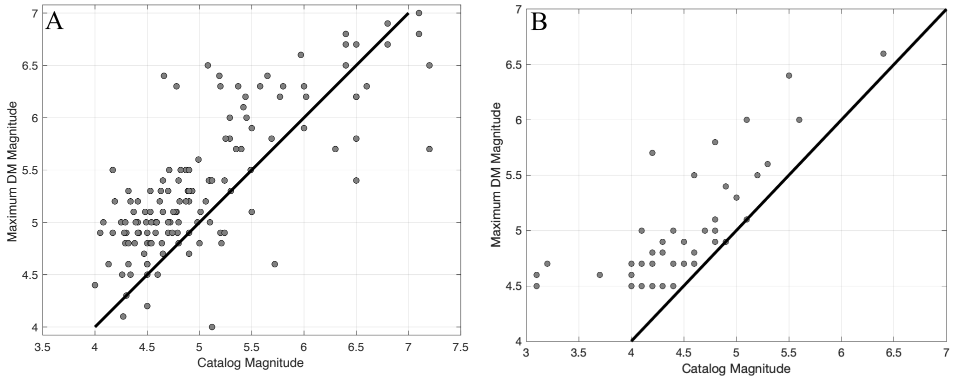

Figure 5. A) Peak DM magnitude for offline replays of the West Coast test suite with V3. For earthquakes with maximum DM magnitudes between 4.5 and 6.0, the median positive bias in maximum estimated magnitude is 0.41 units. B) Peak DM magnitude for real time results for earthquakes in CA that occurred between 1/1/2022 and 2/26/2024 using various versions of the ShakeAlert system that had a maximum magnitude above M4.5. The median positive bias in the maximum estimated magnitude is 0.4 units.

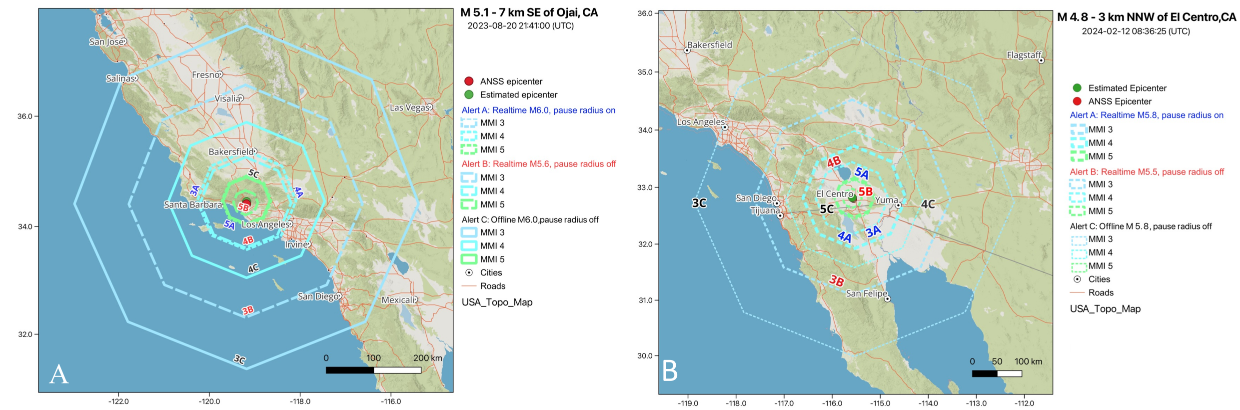

Figure 6: A) Effect of the Alert Pause in the August 20th, 2023, M5.1 Ojai CA earthquake. Contour products are shown for the M6.0 first alert produced by the real-time system, the fourth alert, (~6s after the first alert and M5.6), which produced the largest alert areas. The MMI 3 and 4 contours for the first alert are coincident at 100 km radius as constrained. Also shown are the contours that would have resulted from the M6.0 first alert if the pause radius was not implemented (the largest area polygons). Without the Alert Pause approach, additional MMI 3 alerts would have been sent to San Diego, Fresno, and Salinas (e.g. the region between contour 3B and 3C). Similarly, additional MMI 4 alerts would have been sent to the eastern half of Los Angeles and Santa Barbara (e.g. the region between contours 4B and 4C). B) Effect of the Alert Pause in the 2/12/2024, M4.8 El Centro earthquake. The first alert (A) was M5.8 at 5 seconds after origin time causing the MMI 3 and 4 contours (3A and 4A) to overlap at 100 km radius, after the pause time expired a M5.6 alert (B) was released. If the first alert had been released, cell phone App alerts would have gone to Los Angeles and Riverside CA (region between contours 3B and 3C). Similarly, WEAs would have gone to the suburbs of San Diego (region between contours 4A and 4C).

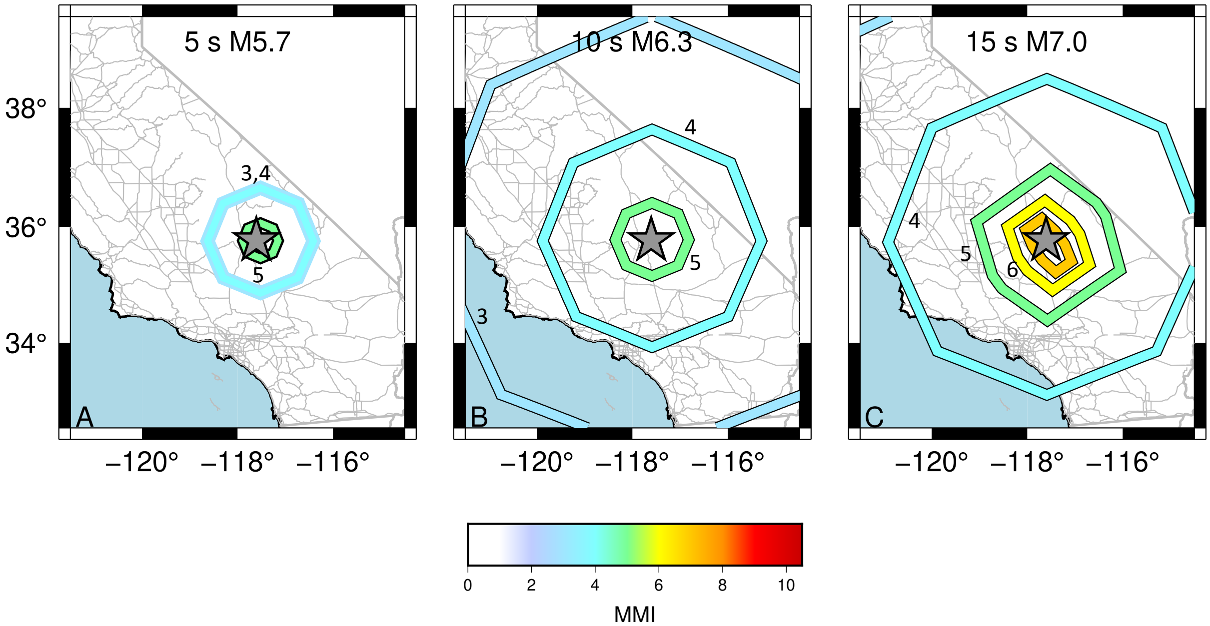

Figure 7. Examples of the temporal evolution of ShakeAlert contour products as the magnitude estimate grows with time during the rupture are shown from an offline replay (with no data delivery latencies included) of V3.0.1 of ShakeAlert for the 2019 Ridgecrest M7.1 earthquake. The MMI 3, 4, 5, and 6 contours are labeled and colored according to the colorbar. A-C) show the evolution of the ShakeAlert MMI estimate polygons corresponding to (A) the initial detection at 5s after the earthquake begins, (B) the moderate-large earthquake stage at 10s, and (C) the large earthquake stage at 15 s. Each map shows several of the contour product polygons for different MMI levels and the ANSS epicenter as a star. In A) the MMI 3 and 4 contour products plot on top of each other at the 100 km pause radius distance, while the MMI 5 contour product is barely visible. In B) the MMI 3, 4, and 5 contour products are visible. In C) the MMI 4, 5, 6, and 7 contour products are visible and the MMI 5-7 polygons are visibly elongated along the fault direction as estimated by the FinDer line source. The MMI 3 polygon in C) is mostly beyond the scale of the map. Currently alerts would only be delivered to users in the State of California for this earthquake even though the polygons extend into Nevada.

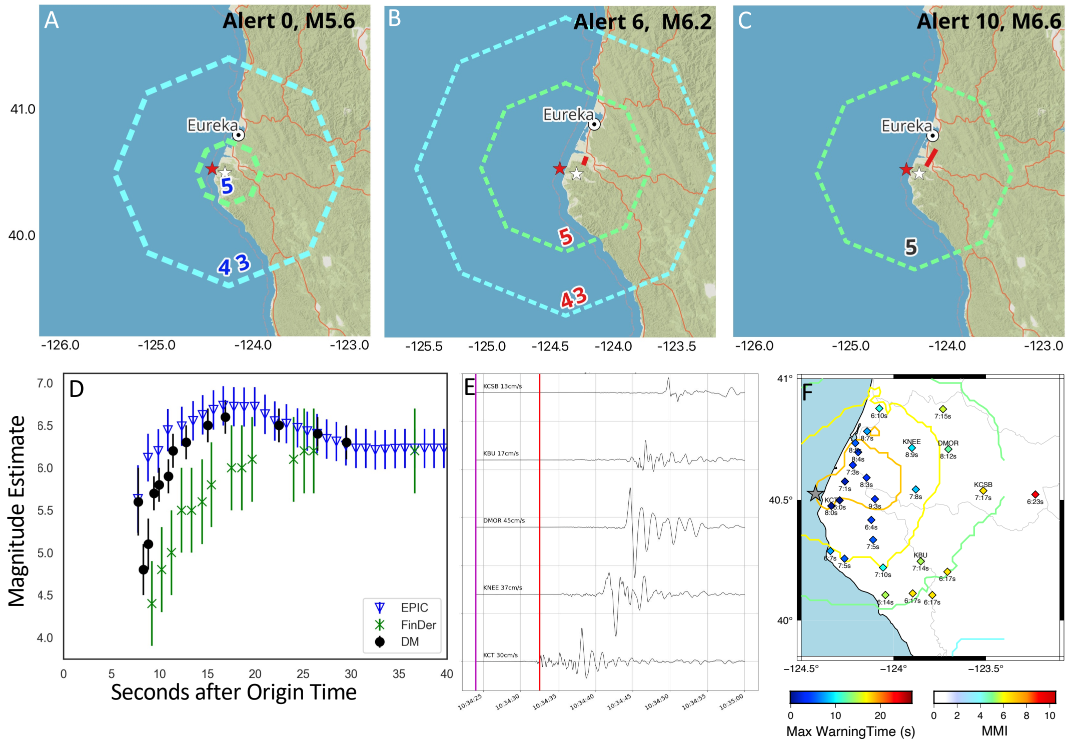

Figure 8: Realtime results from the 2022 M6.4 Ferndale earthquake. A-C) Maps of the first ShakeAlert Contour Message, the 6th update, and the 10th update respectively. The MMI 3, 4, and 5 contour products are shown with the MMI color scale. In panels A and B, the MMI 3 and 4 contours are coincident due to the pause radius. In Panel C, the MMI 3 and 4 contours are beyond the edge of the map. The EPIC epicenter and FinDer line source estimates are shown with red stars and lines respectively. D) Magnitude estimates as a function of time from the production system for the EPIC, FinDer, and DM algorithms. E) Examples of horizontal component seismograms for high amplitude stations. Each station shows the N-S component of ground velocity and is labeled with its station code and peak velocity. F) Map of the epicenter (star) and station locations (diamonds). Light gray lines denote major roads. Each station is labeled with its peak MMI value and warning time (e.g. 7:17s means peak MMI of 7 and 17 s maximum warning time without delivery latency). The color scale of the diamonds denotes the warning

time for the MMI 4 contour product before MMI 5.5 shaking began. Contours show regions of different MMI levels and are colored according to the usual ShakeMap color table for MMI.

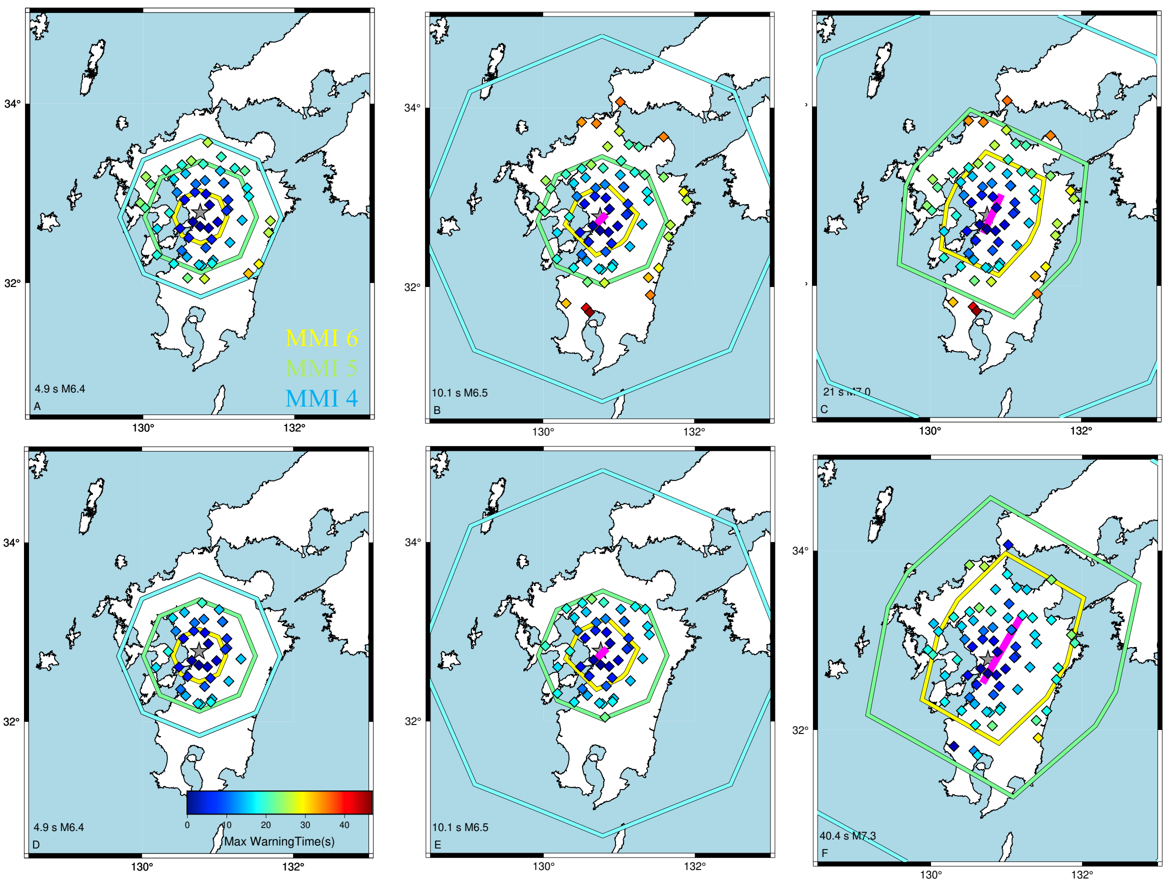

Figure 9. Progression of the MMI 4, 5, and 6 contour products during an offline simulation of the 2016 M7.1 Kumamoto earthquake (star denotes the ANSS epicenter estimate). Panels A, B, and C show warning times before MMI 6 shaking from the MMI 4 contour product at individual stations (diamonds). Only the seismic stations that had peak shaking of MMI 6 or higher are shown. The warning time color scale is the same in all panels. Each panel shows the MMI 4 (light blue), MMI 5 (green) and MMI 6 (yellow) contour products. Each panel is labeled with the seconds after origin time that the DM published the ShakeAlert Message and the associated magnitude estimate. Panels D, E, and F similarly show warning times before MMI 6 shaking from the MMI 5 contour product at individual seismic stations (diamonds). For each panel, only the stations that have been alerted by that contour product at that time are shown. The first alert

(panels A, D) is for a point source as estimated by EPIC. The later alerts at 10.1 s (panels B, E), 21 s (panel C), and 40 s (panel F) show the SA combination of EPIC and FinDer. Because these three estimates are above magnitude 6.0, they include the effect of the FinDer line source (shown as a purple line). While the MMI 5 contour product for the largest alert is sufficient to contain all the MMI 6+ sites, its slower expansion results in reduced warning times compared to those for the MMI 4 contour product (e.g. the difference between panels C and F).

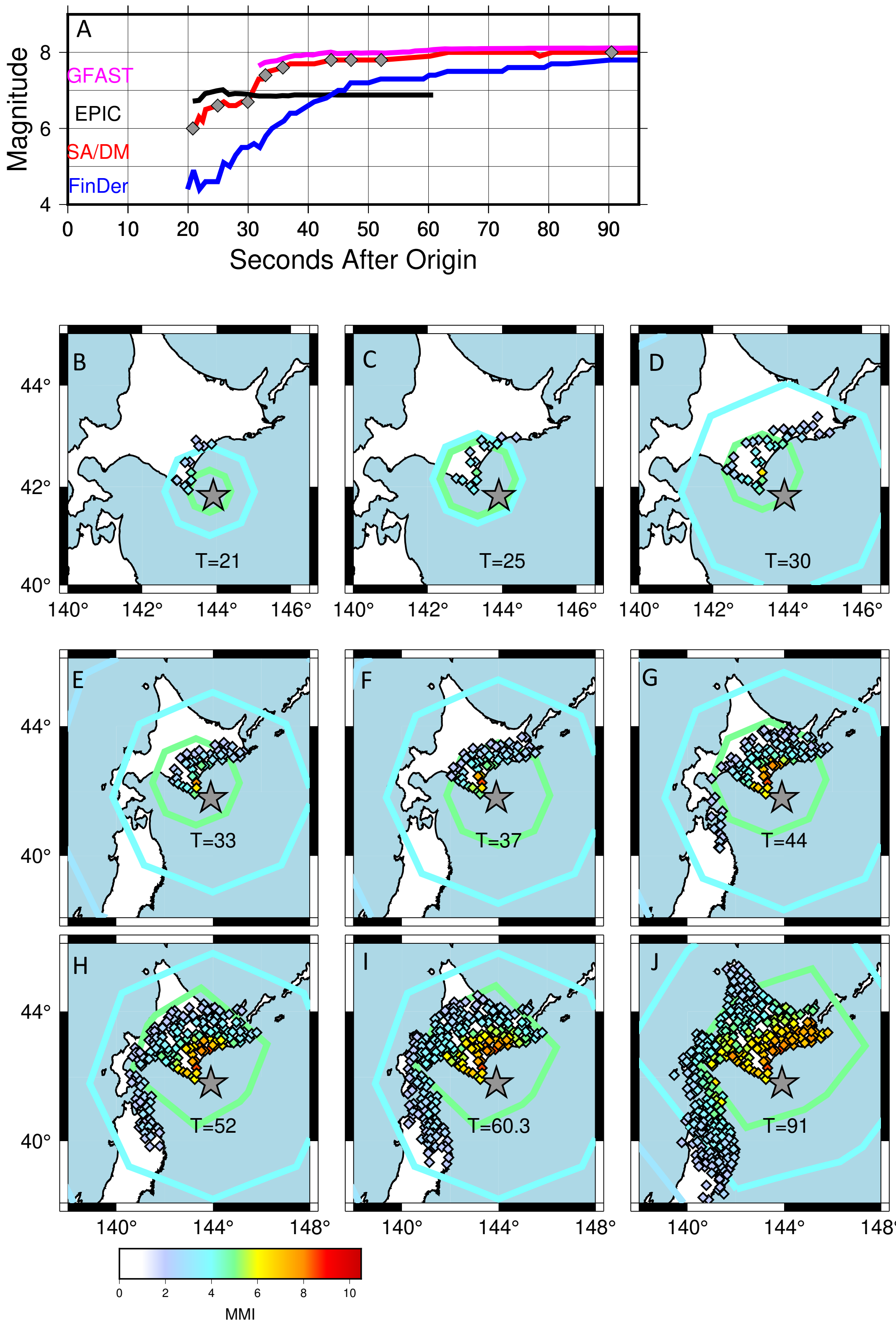

A
Magnitude
GFAST
EPIC
SA/DM
FinDer
Seconds After Origin
B
C
D
E
F
G
H
I
J
T=21
T=25
T=30
T=33
T=37
T=44
T=52
T=60.3
T=91
MMI

1822

Figure 10. Evolution of the magnitude estimates and alerting polygons for an offline replay of V3 for the 2003 M8.3 Tokachi-Oki megathrust subduction earthquake. A) The black, blue, magenta, and red curves show the magnitude estimate evolution from the EPIC, FinDer, GFAST, and SA/DM algorithms respectively. The gray diamonds denote the 9 alerts shown in panels B-J. B-J) Each panel shows the MMI 3, 4, and 5 contour product polygons colored according to the MMI scale and the ANSS epicenter estimate (gray star). Each panel is labeled with the number of seconds after origin time that the DM published the ShakeAlert message (e.g. T=25 is 25 seconds after origin). In panels B and C, the MMI 3 and 4 polygons are coincident due to the Alert Pause and the MMI 3 polygon is completely beyond the bounds of the map in panels H and I. Each small diamond in panels B-J denotes the location of a seismic station used in the simulation and the color denotes the peak MMI value it has reached by that alert's time since origin. The MMI 5 contour is elongated in the along-strike direction because of the FinDer line source estimate. The MMI 5 contour is also slightly offset relative to the MMI 4 contour because the line source estimate is located onshore.

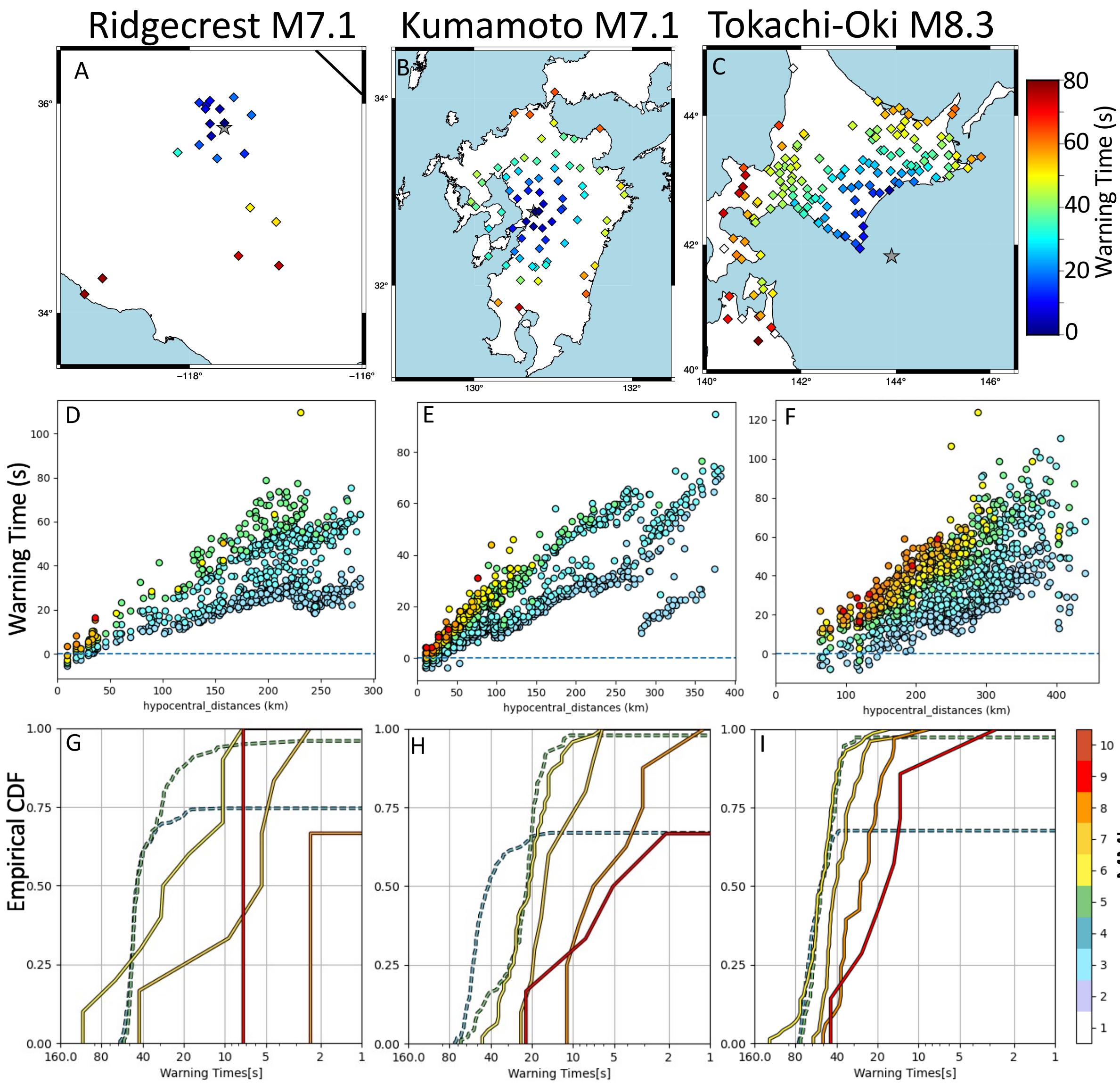

Figure 11: Warning time performance of V3 in offline testing of the 2019 M7.1 Ridgecrest (panels A, D, G), 2016 M7.1 Kumamoto (panels B, E, H), and 2003 M8.3 Tokachi-Oki (panels C, F, I) earthquakes. All results are for the MMI 4 contour product from offline testing without data or delivery latencies. Panels A, B, and C show the warning times between when the MMI 4 contour product is published for that location and when that seismic station recorded MMI 5.5 (diamonds). Gray stars denote the earthquake epicenter. Panels D, E, and F show the temporal evolution of

shaking at each seismic station relative to the time that location was first within the MMI 4 contour product in a ShakeAlert Message. Each station is represented as a vertical series of circles that are colored by MMI level from 2 up through the highest MMI level reached at that location. The colors are denoted by the bar adjacent to panel I. In general, warning times increase with distance from the hypocenter, but this is not monotonic because of the pause radius and the temporal evolution of magnitude estimates during the growing rupture. For some earthquakes, the warning times can be shorter at large distances (e.g. panels D and E at ~250 km) due to the temporal history of the predicted ground motions. Panels G, H, and I show cumulative distributions of warning times for groups of stations binned by their peak MMI level. All of the stations with a peak shaking between MMI 5.5 and 6.5 are shown as the yellow lines with the y-axis indicating the fraction of those stations that achieved the value of warning time along the x-axis. Only seismic stations that recorded MMI 5.5 or larger shaking are shown in the solid lines. Dashed lines for lower MMI locations are based on theoretical S-wave arrival times (see Chung et al., 2020). In general, the higher the peak shaking level, the lower the average warning time but this is not a hard rule as there is considerable overlap in the range of warning times for the different bins of peak shaking (e.g. the MMI 6, 7, 8, and 9 bins all have locations with 40 s of warning time in panel I).

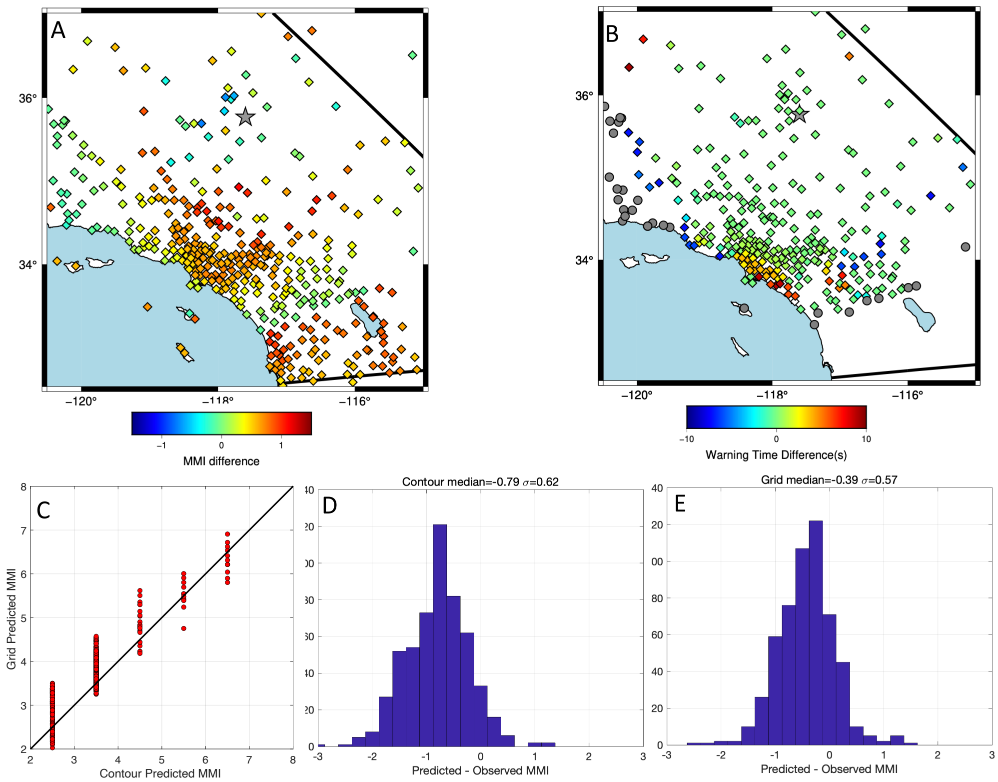

Figure 12. Comparison of the contour and grid (map) product MMI predictions for the offline replay of the Ridgecrest M7.1 including the site response model in the grid product. A) Difference in peak MMI (grid - contour) at the location of seismic stations used in the simulation. B) Warning time differences between the grid product and contour products (grid - contour) using MMI_{alert}=3.5 in the Ridgecrest M7.1 mainshock. Positive differences indicate longer warning times with the grid product. C) Comparison of peak MMI values between the grid and contour products. D) and E) show differences between the predicted and observed peak MMI values using the contour and grid product respectively. The grid product has both a lower median residual and a smaller standard deviation (sigma) of residuals demonstrating its increased accuracy and precision. All predicted values in panels A, C, D, and E use the maximum shaking predicted at a site regardless of timeliness.

1877

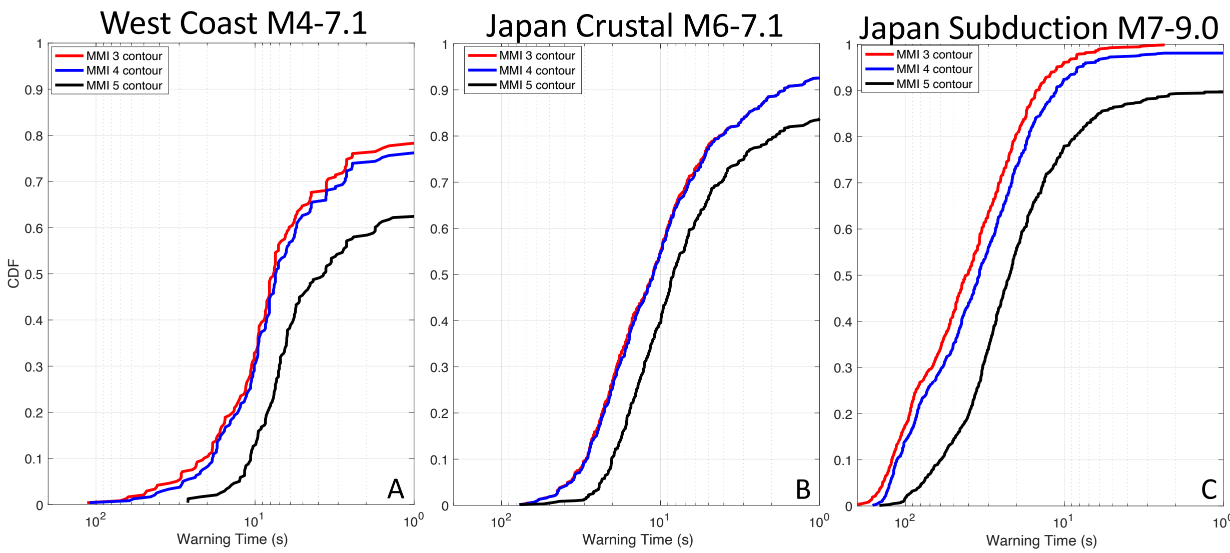

Figure 13: Empirical CDFs of cumulative warning times at seismic stations before strong shaking at 238, 704, and 948 MMI 6+ sites for the west coast (panel A), Japan Crustal (panel B) and Japan subduction zone (panel C). Results for the MMI 3, 4, and 5 contour products are shown as red, blue, and black curves respectively. The magnitude range is lowest for the West Coast dataset (M4.0 - 7.1) leading to shorter overall warning times than the Japan Crustal (M6.0-7.1) and Japan Subduction Zone (M7.1-9.0). Additionally, most of the subduction events begin offshore where there are no seismic stations, and thus, there are no measurements in the late alert zone for that panel.

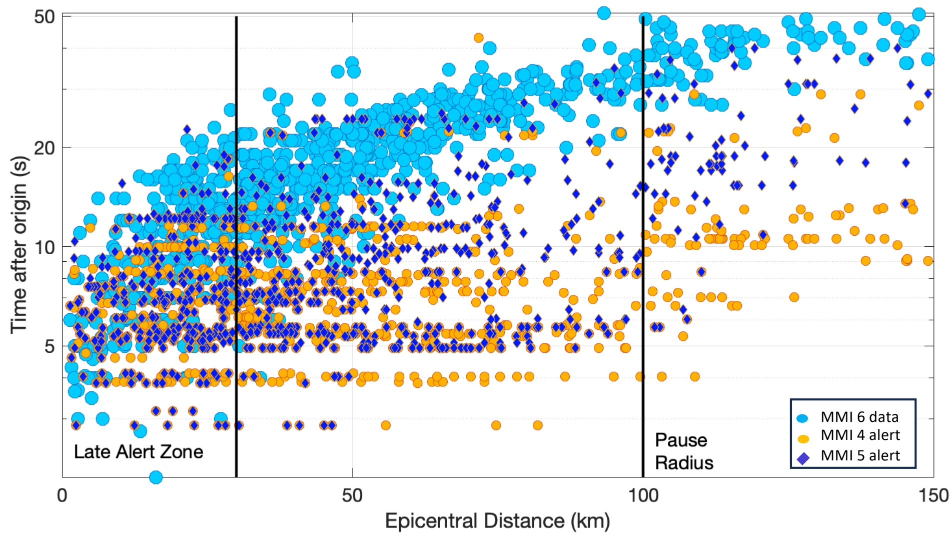

Figure 14. Comparison of the time that strong shaking begins with the time of MMI 4 and 5 contour product alerts for the shallow crustal earthquakes in the West Coast and Japan crustal datasets. Light blue circles denote the time that MMI 5.5 shaking began at individual seismic stations. Orange circles and dark blue diamonds denote the time that those same seismic stations were first alerted with the MMI 4 and 5 contour products respectively. Vertical lines at 30 km and 100 km epicentral distance denote the approximate location of the extent of the late alert zone and the pause radius respectively. Note the epicentral distances are with respect to the ANSS catalog epicenter, not the ShakeAlert epicenter estimate that controls the calculation of the pause radius. The Y-axis is a log scale. At a given epicentral distance range, say 50-60 km, the MMI 6 exceedance time (light blue circles) can vary over about 15-20 seconds due to many factors related to how a particular earthquake ruptures. The times the MMI 4 and 5 contour product were published are from offline simulations and do not include the latencies associated with data telemetry or alert delivery which would typically add a minimum of 2 seconds to these times and can vary widely between delivery mechanisms.

1905

1906

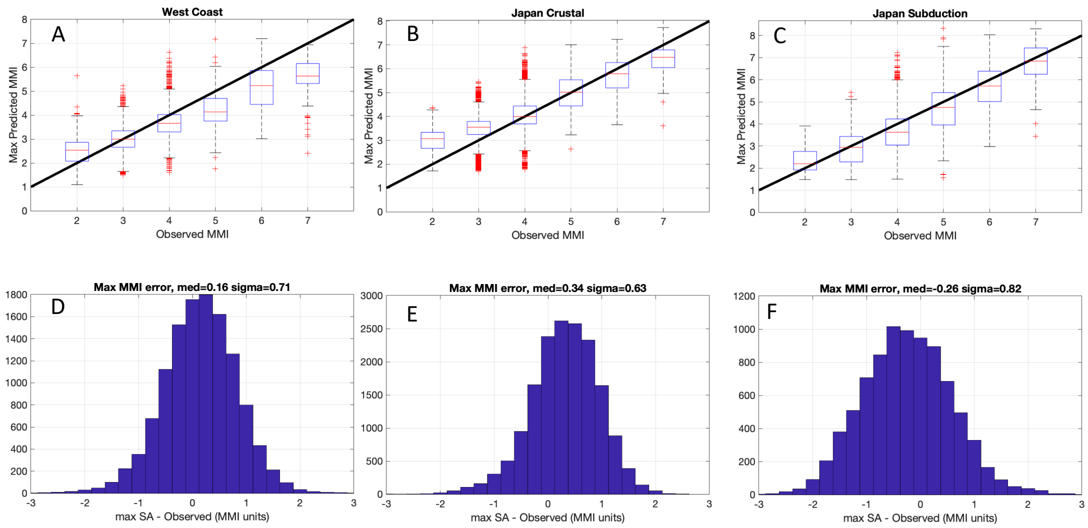

Figure 15: Comparison of individual station maximum predicted and observed MMI values for the West Coast (A, D), Japan Crustal (B, E), and Japan Subduction Zone (C, F) testing datasets. All predicted values are from the map products. Panels A, B, and C show all predictions in one MMI bins and the 25 and 75th percentiles (box) as well as large outliers (red whiskers). Panels D, E, and F show individual station residuals which are dominated by MMI 2-4 levels in these datasets. Each panel gives the median and standard deviation of the residuals. These maximum predicted values encompass the performance of the entire system including the magnitude over and under estimates in individual earthquakes. In general, ShakeAlert is unbiased for all three datasets with the exception of underpredicting the highest MMI 5-7 sites in the West Coast dataset.